Miki(ΔN) protein (Figure 3F, lane 3) can be PARsylated in vitro by tankyrase-1 immunoprecipitated from HeLa cells (lane 17). However, PAR immunoblot analysis of Miki immunoprecipitates revealed that Miki(ΔN) is not PARsylated in vivo (Figure 3J, lane 2). This is different from the full-length Miki, which, as expected, shows a strong $p125^{Miki}$ band (lane 3). Consequently, not only siRNA#79 but also siRNA#80 reduced the levels of $p125^{Miki}$ in cells expressing Miki(ΔN) (Figure 3K, lanes 4 and 5), resulting in a significant increase of the proportion of cells in pseudometaphase by both siRNA#79 and siRNA#80 (Figure 2H).

Downregulation of Miki Reduces the Robustness of Spindles

To investigate the mechanism(s) through which Miki downregulation causes prometaphase disturbance, we monitored the movement of lagging chromosomes in pseudometaphase relative to those in normal late prometaphase. In control siRNA-treated U2OS cells expressing H2B-GFP, all lagging chromosomes in late prometaphase moved toward the metaphase plate at a velocity greater than 1 μm/min, typically 2–5 μm/min (Figure 4A, open bars), consistent with previous reports (Gordon et al., 2001; Levesque and Compton, 2001). In contrast, nearly half of the lagging chromosomes in pseudometaphase cells resulting from siRNA#80 treatment moved less than 1 μm/min (black bars).

Chromosomes may move slowly due to insufficient microtubule tension at kinetochores caused by unfixed (highly motile) spindle poles resulting in synchronous rotation of the chromosomes at prometaphase (Movie S2 and Movie S3) and loss of robustness of mitotic microtubules. α-tubulin staining of siRNA#80-treated cells revealed curling and disorganized spindles, with an occasional chaotic centrosome at only one side of the alignment (Figure 4B). Although spindle microtubules were not visibly fragile, the ratio of tubulin polymers to dimers, a more sensitive measure of spindle strength (Mishima et al., 2004), was reduced to 52% following siRNA#80 treatment for 48 hr compared with cells treated with control siRNA (Figure 4C, compare panel 2 with panel 1). Moreover, low concentrations (1 μM) of nocodazole, a microtubule depolymerizer or short-term cold treatment (5 min) that did not visibly affect mitotic spindles of control cells (compare panels 3 and 5 with panel 1), markedly degraded mitotic spindles of siRNA#80-treated cells (panels 4 and 6).

These findings suggest that Miki downregulation impairs critical a centrosome function(s) such as microtubule nucleation. As demonstrated previously by others (Vaughan, 2005), accumulation of the EB1 microtubule tip-binding protein at centrosomes indicates active microtubule nucleation during mitosis (Figure 4D, panel 1, arrows). The MMC culture method revealed that treatment of HeLa cells with siRNA#80 induced mitotic cells with a pseudometaphase phenotype with markedly reduced centrosomal EB1 signals (panel 2, right-hand cell).

Reduced microtubule nucleation in response to Miki downregulation was also demonstrated in microtubule regrowth assays. Mitotic spindles degraded completely by simultaneous treatment of cells with nocodazole and cold (Figure 4E, panel 1). At this time point, mitotic centrosomes, which are shown as a pair of green dots by γ-tubulin staining (lower right), had several-fold higher intensities than nearby interphasic centrosomes (arrows), as a result of centrosome maturation (discuss in the next section). The cells were then cultured in nocodazole-free medium at 37°C. Within 5 min, 32% of control siRNA-treated mitotic cells showed small asters (<5 μm) forming at centrosomes (panel 2); 8 min later, large asters (>5 μm, panel 3) were observed in 50% of mitotic cells, and numbers increased to nearly 100% within 15 min (panel 4 and bar graph). In contrast, siRNA#80-treated mitotic cells had weaker γ-tubulin signals in centrosomes than cells in interphase (panel 5) and frequently formed multiple small asters (panel 7), and only 16% of mitotic cells showed large asters after 15 min.

The reduced signals of γ-tubulin in mitotic centrosomes and delays of microtubule extension induced by Miki siRNA#80 were rescued by the forced expression of the full-length Miki (panels 9–12), but not by Miki(ΔN) (panels 13–16).

Insufficient Centrosome Maturation Due to Miki Downregulation

The above findings imply that Miki downregulation might impair the γ-tubulin ring complex (γ-TuRC) localizing to the pericentriolar matrix (PCM) that scaffolds microtubule nucleation sites at mitotic centrosomes. Major components of γ-TuRC accumulate in mitotic centrosomes during the short period from late G2 to prometaphase known as "centrosome maturation." For example, the intensity of γ-tubulin immunostaining in prometaphase centrosomes of HeLa cells treated with control siRNA (Figure 5A, arrowheads) increased several-fold relative to those at interphase (arrows). Similarly, other major components of γ-TuRC such as GCP2, kendrin/pericentrin, and CG-NAP/AKAP450 accumulated in mitotic centrosomes (right panel).

To test whether Miki downregulation by siRNA#80 affects signal intensities of these four γ-TuRC components in interphase centrosomes, we transfected Cy3-labeled siRNA#80 into HeLa cells. Prometaphase disturbances including pseudometaphase were induced by Cy3-labeled siRNA#80 and unlabeled siRNA#80 at a similar frequency (data not shown). The intensity of γ-tubulin signals in interphasic centrosomes of Cy3-positive cells (Figure 5B, upper two cells) was essentially the same as in Cy3-negative cells (lower two cells). Indeed, Miki downregulation did not affect signals from four major components of γ-TuRC in interphasic centrosomes (right panel),

(D) U2OS cells that express a histone H2B-GFP fusion protein constitutively were treated with the siRNA (100 nM, indicated at left) for 36 hr. Cells (200 each) that entered prophase were observed for 12 hr.

(E) HeLa cells were treated for 48 hr (for anexinV) or 72 hr (for caspase-3 and TUNEL assay) as indicated at left. Shown is average with SD (four independent experiments) of the percentage of cells positive for annexin-V staining, high caspase-3 activity, or TUNEL assay.

(F) HeLa cells were treated with Miki siRNA#80 for 72 hr. DNA was stained with Hoechst 33342.

(G) Shown are Miki or β-actin antibody immunoblots of HeLa cells (lane 1), cells expressing $Miki^{MT80}$ (lanes 2–5) treated with control siRNA (lane 3), siRNA#79 (lane 4), or siRNA#80 (lane 5). Arrows indicate position of p125, p50; bracket, glycosylated exogenous Miki protein; asterisk, unidentified bands.

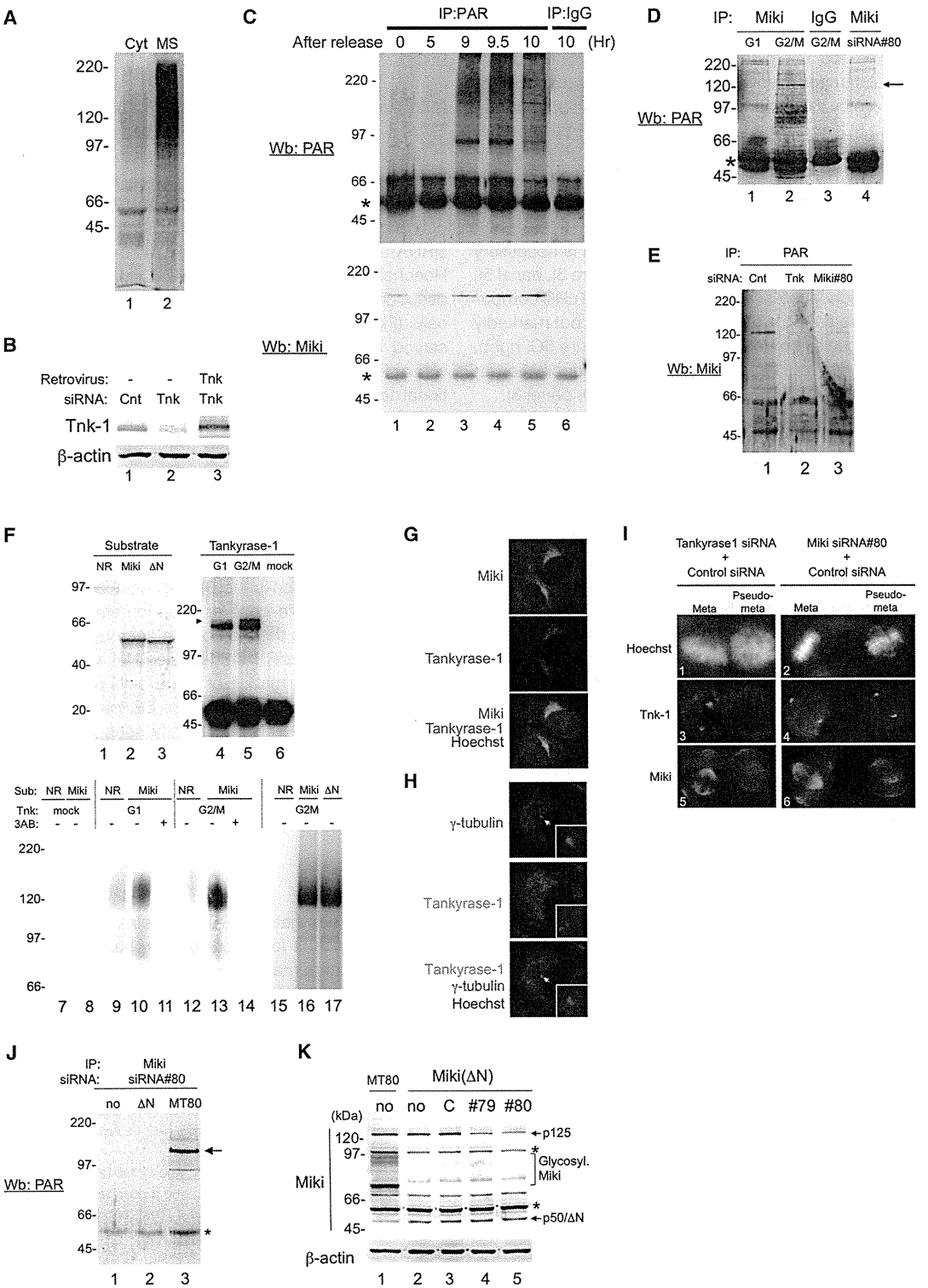

Figure 3. PARsylation of Miki by tankyrase-1

(A) PAR antibody immunoblots of the cytosolic fraction (Cyt) and isolated mitotic spindles and centrosomes (MS) from an equal number of cells.

(B) Immunoblot analysis using tankyrase-1 and β-actin antibodies of whole-cell lysate from HeLa cells (lanes 1 and 2) and cells infected with MSCV-tankyrase-1 (lane 3) treated with control siRNA (lane 1) or siRNA for tankyrase-1 (lanes 2 and 3) (200 nM each for 72 hr).

consistent with the fact that Miki is not present in interphasic centrosomes (Figure 1B).

In contrast to the situation with interphasic centrosomes, Miki downregulation reduced γ-tubulin signals in mitotic centrosomes, as shown by a comparison between those in pseudometaphase (Figure 5C, arrowheads) and those in a nearby interphasic centrosome (arrow). In addition, Miki reduced GCP2 and CG-NAP levels in centrosomes of pseudometaphase even to below those in interphase cells, and prevented the accumulation of kendrin (right panel).

Similarly, downregulation of tankyrase-1, which is necessary for Miki accumulation in mitotic centrosomes (Figure 3I, panel 5), did not affect immunofluorescence signals from γ-TuRC components in interphase centrosomes (Figure 5B, right) but markedly reduced these signals in mitotic centrosomes (Figure 5C, right). Subsequently, tankyrase-1 reduced microtubule nucleation at mitotic centrosomes monitored by EB1 (Figure 4D, panel 3).

To identify the critical γ-TuRC component(s) required for prompt chromosome alignment by PARsylated Miki, we downregulated each component separately by siRNA. CG-NAP downregulation (Figure 5D) caused a significant increase of cells with a pseudometaphase phenotype, in which accumulation of EB1 signals in mitotic centrosomes was not evident (Figure 4D, panel 4). However, the MMC culture method revealed that reduction of CG-NAP did not affect localization of Miki (Figure 5E, panel 5) and tankyrase-1 (panel 6) in mitotic cells. This suggests that CG-NAP is a downstream target of PARsylated Miki to promote progression of prometaphase. In contrast, cells expressing kendrin at reduced levels showed mostly monopolar spindles (data not shown), as previously described by others (Zimmerman et al., 2004), and no significant increase in pseudometaphase (2/200). We could not successfully downregulate γ-tubulin and GCP2.

Finally, we identified ch-TOG/XMAP215, a processive microtubule polymerase (Brouhard et al., 2008) localized to mitotic centrosomes/spindles (Figure 5F, left-hand cells) as a downstream target of PARsylated Miki and CG-NAP. Like major components of γ-TuRC, downregulation of Miki, tankyrase-1, or CG-NAP did not affect fluorescent signal intensity of ch-TOG in interphase centrosomes, but all inhibited accumulation of ch-TOG in mitotic centrosomes (Figure 5G). Conversely, siRNA-mediated downregulation of ch-TOG (Figure 5F, middle panels) did not inhibit centrosomal accumulation of Miki or tankyrase-1 (bottom panels) but caused an increase of prometaphasic cells and pseudometaphase phenotypes to a high frequency (Figure 2C), as predicted by a previous report (Gergely et al., 2003).

Miki Downregulation in Normal Human Primary Cells

To test whether Miki promotes progression of prometaphase in untransformed cells, we downregulated its expression using siRNA#80 in primary cutures of normal human tissues such as retinal pigment epithelial (hRPE) cells (Figure 6A). The number of floating mitotic cells significantly increased from 3.7% (control siRNA-treated cells) to 11.7% (siRNA#80-treated cells) ($p < 0.01$). Hoechst 33342 staining revealed that siRNA#80 induces pseudometaphase (Figure 6B, panel 4) in roughly 6% of mitotic cells (Figure 6C), while no typical pseudometaphase was observed in cells treated with control siRNA. In addition, there was a significant increase of cells at prometaphase and a proportional decrease of those at metaphase, anaphase, and telophase.

Immunostaining revealed that Miki localizes to mitotic spindles in control-siRNA treated hRPE cells (Figure 6B, panel 2). However, in mitotic cells with a pseudometaphase phenotype, Miki signals were barely detectable in mitotic centrosomes and nearby spindles identified by γ-tubulin staining (panel 5). The intensity of γ-tubulin staining in metaphasic centrosomes of control siRNA-treated hRPE cells increased several-fold relative to those at interphase (panel 3), but no enhancement of γ-tubulin signals was seen in cells at pseudometaphase (panel 6), although neither was there a notable decrease (Figure 6D), which is characteristic of siRNA#80-treated HeLa cells (Figure 5C). As a result, spindle formation of hRPE cells at pseudometaphase showed mild disturbances (Figure 6E, panel 6), in contrast to the severe abnormalities frequently seen in siRNA#80-treated HeLa cells (Figure 4B).

Except for the hRPE cells, none of the other normal human primary cells we treated with siRNA#80 showed any mitotic disturbance.

DISCUSSION

We demonstrate that two Golgi proteins, tankyrase-1 and Miki, neither of which is localized to interphasic centrosomes, promote centrosome maturation. In late G2 phase, coincident with the fragmentation of the Golgi apparatus, tankyrase-1 is activated by phosphorylation via GSK-3 (Yeh et al., 2006) and PARsylates Miki, which then translocates to mitotic centrosomes/

(C–E) Cell-cycle phase-enriched HeLa cells (C; D, lanes 1–3) or cells treated with siRNAs indivated above (D, lane 4; E) were subjected to immunoprecipitation (IP) using the antibodies indicated above followed by immunoblot analysis (Wb) using the antibodies indicated. IgG, control mouse IgG. Asterisk indicates position of the immunoglobulin heavy chain.

(F) Tankyrase-1 PARP assay. Coomassie-stained gel with purified in vitro translation products from a no-RNA control (NR, lane 1), Miki mRNA (lane 2), or Miki(ΔN) template. Anti-tankyrase-1 immunoprecipitates from lysates of HeLa cells synchronized at G1 (lane 4) or G2/M (lane 5), and a no-lysate control (mock, lane 6). Autoradiography of PARP-labeled products prepared in the presence or absence of purified substrate (Sub), tankyrase-1 (Tnk), and 3 aminobenzamide (3AB, 1 mM), as indicated above (lanes 7–17).

(G–I) Immunostaining of HeLa cells using antibodies indicated at left. Cells were treated with different siRNAs indicated above (I). DNA was stained with Hoechst 33342. Arrowheads show positions of centrosomes; insets, enlargements of a centrosomal area (H).

(J) HeLa cells (lane 1) or cells expressing Miki(ΔN) (lane 2) or full-length Miki (lane 3) treated with siRNA#80 were subjected to immunoprecipitation (IP) using Miki antibodies followed by immunoblot analysis using PAR antibody. Asterisk indicates position of the immunoglobulin heavy chain.

(K) Miki or β-actin antibody immunoblots of HeLa cells expressing $Miki^{MT80}$ (lane 1), cells expressing Miki(ΔN) (lanes 2–5) treated with control siRNA (lane 3), siRNA#79 (lane 4), or siRNA#80 (lane 5). Arrows indicate position of p125, p50 or Miki(ΔN); bracket, glycosylated exogenous Miki protein; asterisk, unidentified bands.

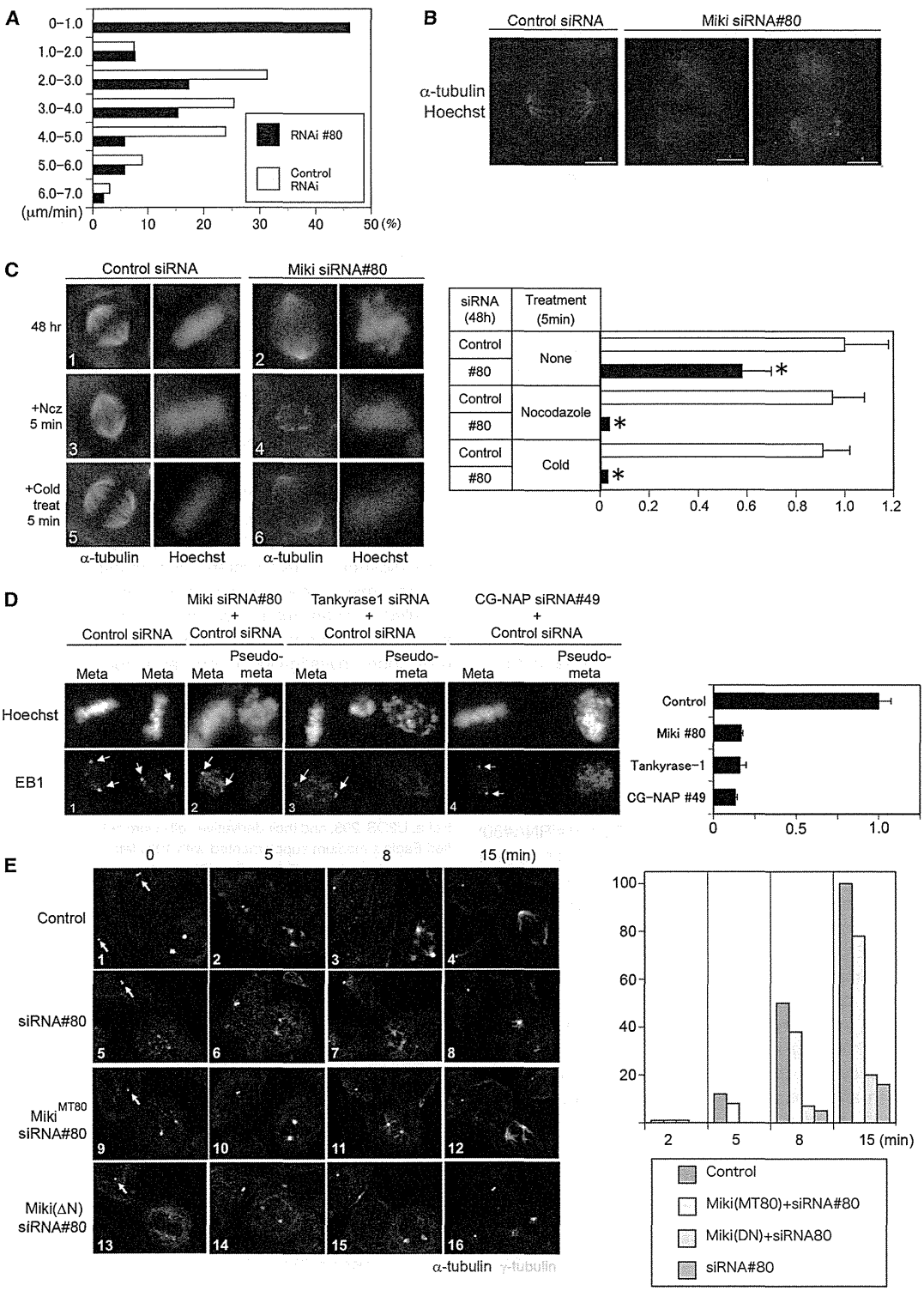

Figure 4. Fragility of Mitotic Spindles in Cells Expressing Low Levels of Miki

(A) Histogram representing the percent (x axis) of H2B-GFP-expressing U2OS cells treated with either 100 nM control siRNA (open bars) or siRNA#80 (black bars) in each 1 μm/min category of lagging chromosome velocity (at left). For calculations of maximum velocity (μm/min), photographs were taken every 15 s over each 15 min observation period.

spindles. Analysis using the Miki(ΔN) mutant revealed that localization of Miki in the Golgi apparatus is necessary for PARsylation and translocation to mitotic centrosomes and spindles.

During the process of centrosome maturation, components of γ-TuRC are rapidly transported and anchored to centrosomes through divergent pathways (for review, see Blagden and Glover, 2003). γ-tubulin, GCP2, and/or GCP3 form a complex called the small γ-TuRC (γ-TuSC) in the cytosol, whereas CG-NAP and kendrin, cognate giant scaffold proteins that share coiled-coil structures, are transported to centrosomes by the dynein/dynactin motor complex. γ-TuSC is then anchored to centrosomes through association of GCP2/GCP3 with CG-NAP/kendrin to form γ-TuRC (Keryer et al., 2003; Takahashi et al., 2002).

Although CG-NAP and kendrin form a complex to provide a platform for γ-TuRC, the roles of each protein are likely to differ because specific suppression of CG-NAP by siRNA disturbs prometaphase through loss of microtubule nucleation, whereas kendrin downregulation causes monopolar spindle formation (Zimmerman et al., 2004). In addition, we recently reported that CG-NAP is connected with the centrioles by interacting with Cep72 (centrosomal protein 72 kDa) (Oshimori et al., 2009). The latter is a previously uncharacterized protein that forms complexes with Kizuna to maintain the integrity of mitotic centrosomes and protect PCM from fragmentation by microtubule-mediated forces (Oshimori et al., 2006). These data suggest that CG-NAP, rather than kendrin, provides a platform for localizing γ-TuRC near centrioles. Downregulation of tankyrase-1 or Miki reduces CG-NAP to barely detectable levels in mitotic centrosomes, while kendrin is maintained at levels similar to those in interphase centrosomes (Figure 5C). This suggests that Miki mainly contributes to CG-NAP-mediated γ-TuRC formation and subsequent microtubule nucleation processes that promote progression of prometaphase.

Severe disturbance of prometaphase was readily induced by Miki downregulation using two siRNAs (siRNA#79 and siRNA#80) or short-hairpin RNA (Asou et al., 2009), each of which targets a different sequence in different human cancer cell lines including HeLa, U2OS, and K562 leukemia cells. We also treated a series of human primary cells with siRNA#80 but found that of these, only hRPE cells showed definite but still relatively mild disturbances at prometaphase (Figure 6). In addition, mice lacking the *Miki* gene do not show apparent abnormalities, and cell lines established from them divide normally (our unpublished data using mice that we generated).

These differences in the effects of Miki downregulation between human and mouse cells or between cancer and untransformed cells suggest that the essential function of Miki anchoring γ-TuRC to mitotic centrosomes can be to a greater or lesser extent substituted by another factor(s). Indeed, members of γ-TuRC including γ-tubulin are readily detected by immunostaining in interphasic centrosomes (Figure 5A) where tankyrase-1 and Miki appear to be absent. Miki downregulation reduces γ-tubulin in mitotic centrosomes to barely detectable levels in HeLa cells (Figure 5C), whereas γ-tubulin in siRNA#80-treated hRPE cells under pseudometaphase conditions is maintained at levels of interphasic centrosomes (Figures 6B, 6D, and 6E), though not enhanced. These findings suggest that HeLa cells may have lost a tankyrase-1/Miki-independent mechanism(s) to anchor γ-TuRC to mitotic centrosomes.

Alternatively, cancer cells may harbor defects of multiple factors in the tankyrase-1/Miki-dependent system for centrosome maturation. For instance, as we previously reported (Asou et al., 2009), low Miki expression levels in MDS cells relate to so-called colchicine-mitosis (scattered and lagging chromosomes) and subsequent abnormal nuclear morphology (binuclei, trinuclei, or multiple nuclei with micronuclei) that characterize MDS. Intriguingly, the CG-NAP gene (1.2 Mb centromeric to *Miki* in band 7q21) also maps to a region frequently deleted in MDS; ~20% of MDS patients lose one allele of both *Miki* and *CG-NAP* genes. This indicates that loss of chromosome arm 7q results in low expression of two crucial factors in the tankyrase-1/Miki-dependent system for centrosome maturation, and that this may profoundly impair progression of prometaphase. Detailed mechanisms through which impairment of the tankyrase-1/Miki-dependent system perturbs cancer cell mitosis are now under investigation in our laboratory, because abnormal mitosis directly causes chromosome instability that could determine the fate of cancer patients.

EXPERIMENTAL PROCEDURES

Cell Culture and Gene Transfer

HeLa, U2OS, 293, and their derivative cells were cultured in Dulbecco's modified Eagle's medium supplemented with 10% fetal bovine serum. hRPE cells were purchased from Takara Bio. (Ohtsu, Japan) and cultured according to the manufacturer's directions. The siRNA oligonucleotides for Miki siRNA#79, siRNA#80, and siRNA#81 (Asou et al., 2009); tankyrase-1 (Dynek and Smith, 2004); ch-TOG (Gergely et al., 2003); NuMA (Chang et al., 2005b) or CG-NAP (siRNA#49, 5′-GCUUCUAUUUAGUCACGAA-3′) were transfected into HeLa(tc) (Oshimori et al., 2006), U2OS, or hRPE cells using Oligofectamine (Invitrogen). Pantropic retrovirus was generated according to procedures described elsewhere (Ozaki et al., 2011) using pMSCV (Clontec) and ires-CD8 (Kuribara et al., 1999).

Mixed Mitotic Cell Culture for Immunostaining

Comparison of immunofluorescence signal intensity between cells treated with different siRNAs was performed as follows. Mitotic cells treated with specific siRNA (for Miki, tankyrase-1 or CG-NAP, which causes mitotic arrest)

(B) Immunostaining of HeLa cells treated with the siRNA indicated above using α-tubulin antibody. DNA was stained with Hoechst 33342.

(C) HeLa cells cultured in the presence of control siRNA or siRNA#80 (100 nM each) for 48 hr (top) were treated with 1 μM nocodazole for 5 min (middle), or put on ice for 5 min (bottom) before immunostaining with α-tubulin antibodies. DNA was stained with Hoechst 33342. The average ratio (20 cells) of tubulin polymers to dimers (with SD) is shown on the right.

(D) Immunostaining of HeLa cells treated with the siRNA indicated above using EB1 antibody. DNA was stained with Hoechst 33342. Relative fluorescence intensity (with SD) (100 centrosomes) is shown at right.

(E) Microtubule regrowth assay. HeLa cells (treated with siRNA and transfected with retrovirus indicated at left) were cultured at low temperature and treated with nocodazole to degrade spindles (0 min), then cultured without nocodazole at 37°C for the periods indicated above (α- and γ-tubulin staining). The ratio of mitotic cells harboring large asters (>5 μm) is shown at right (100 cells).

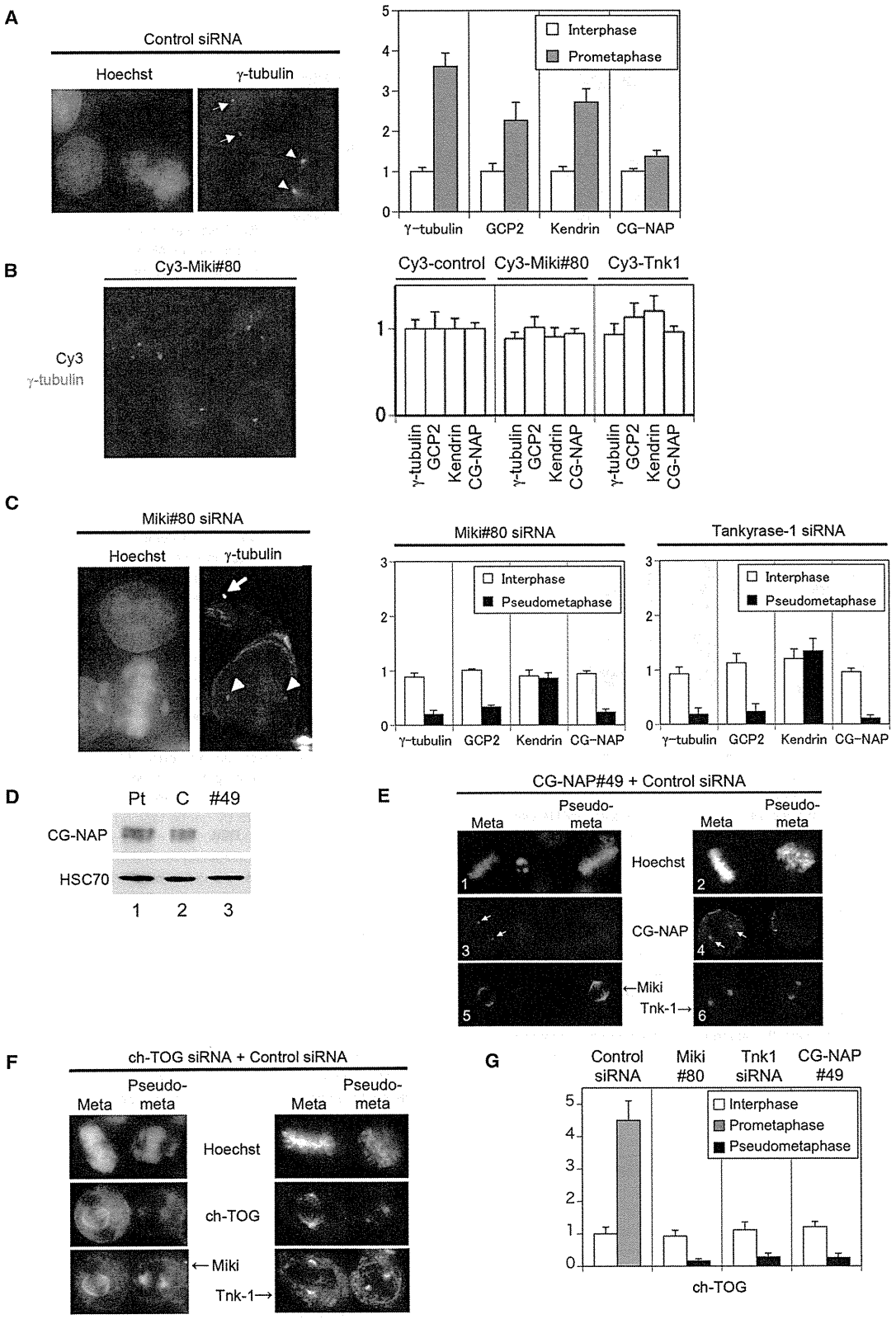
A
Control siRNA
Hoechst
γ-tubulin
Interphase
Prometaphase
γ-tubulin
GCP2
Kendrin
CG-NAP
B
Cy3-Miki#80
Cy3
γ-tubulin
Cy3-control
Cy3-Miki#80
Cy3-Tnk1
C
Miki#80 siRNA
Hoechst
γ-tubulin
Interphase
Pseudometaphase
Tankyrase-1 siRNA
D
Pt
C
#49
CG-NAP
HSC70
1
2
3
E
CG-NAP#49 + Control siRNA
Meta
Pseudo-meta
Hoechst
CG-NAP
←Miki
Tnk-1→
F
ch-TOG siRNA + Control siRNA
ch-TOG
G
Control siRNA
Miki #80
Tnk1 siRNA
CG-NAP #49
Interphase
Prometaphase
Pseudometaphase
ch-TOG

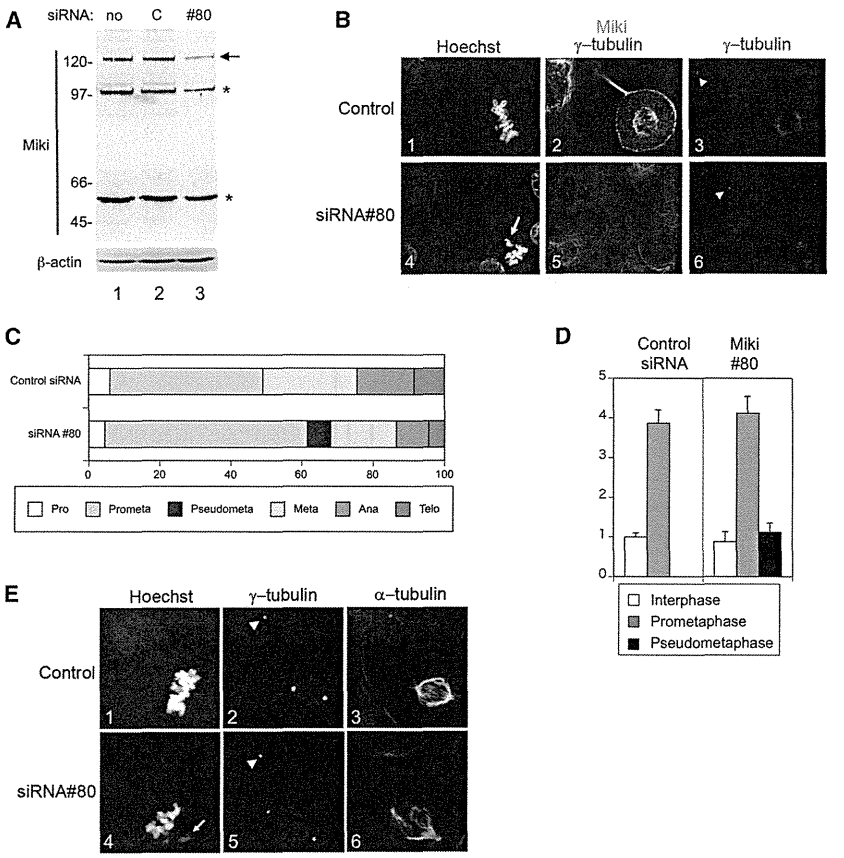

Figure 6. Mitotic Disturbance by Miki Downregulation in hRPE Cells

(A) Miki and β-actin immunoblots of hRPE cells (lane 1), cells treated with control siRNA (lane 2), or siRNA#80 (lane 3) (100 nM for 48 hr). Arrows indicate position of p125; asterisks, unidentified bands.

(B and E) Immunostaining of cells treated with the siRNA indicated on the left using the antibodies indicated above. DNA was stained with Hoechst 33342.

(C) Cells were treated with the siRNA indicated at the left for 48 hr. Percentages of the 500 cells in each mitotic phase or undergoing abnormal mitosis were calculated from observations of Hoechst 33342-stained nuclei. Asterisks indicate significant changes relative to the control.

(D) Relative fluorescence intensity of γ-tubulin in centrosomes at interphase (open bars), prometaphase (gray bar), or pseudometaphase (black bar) in cells treated with the siRNAs indicated above. Shown is average with SD (20 centrosomes).

for 48 hr were detached from the coverslip by gentle pipetting. Detached cells were then added to another coverslip, on which cells had been cultured with control siRNA for 48 hr. After culture for an additional 3 hr, the coverslip containing mitotic cells treated with both specific or control siRNA was immunostained according to methods previously described (Oshimori et al., 2006; Tokai-Nishizumi et al., 2005). Relative fluorescence intensity was measured using ImageJ software.

Tankyrase-1 PARP Assay

A cDNA encoding hexameric His-tagged human Mikiα was cloned into pTD1 (Shimadzu, Kyoto, Japan) and mRNA synthesized in vitro using the Megascript system (Ambion, Foster City, CA). Protein synthesized in vitro using the Transdirect insect cell system (Shimadzu) was purified on Ni-NTA beads. Tankyrase-1 was immunoprecipitated from HeLa cells that had been synchronized at G1 or G2/M phase using the standard double-thymidine method. PARP assays were performed using 1 μg purified Miki, tankyrase-1 bound to protein G beads, and [^{32}P]NAD$^+$ according to the method previously described (Seimiya et al., 2004).

Mitosis Analysis

Floating mitotic cells were counted by detaching cells by gentle pipetting and staining with trypan blue to exclude apoptotic cells. Chromosome velocities were measured in U2OS cells expressing an H2B-GFP fusion protein using methods described previously (Levesque and Compton, 2001). Nocodazole sensitivity and cold tests were performed as described previously (Oshimori et al., 2006; Tokai-Nishizumi et al., 2005). The ratio of tubulin polymers to dimers was quantified based on a procedure described previously (Mishima et al., 2004). Mitotic spindles were isolated according to a previously described method (Sillje and Nigg, 2006). Briefly, synchronized HeLa cells at the G2/M boundary were detached from the plate by gentle tapping and then incubated for an additional 30 min. Cells mostly (>90%) in metaphase or early anaphase were lysed with hypotonic buffer containing taxol and ADP-HDP (30 μM; Merck), a PARG inhibitor. Then, by removing soluble cytosolic and membrane/actin-associated proteins as well as intermediate filaments by centrifugation, mitotic spindles/centrosomes were isolated. Microtubule regrowth assays were performed by completely depolymerizing tubules in cells with 10 mM nocodazole on ice for 60 min. Cells were washed three times with serum-free medium and then incubated in warm medium at 37°C.

Other Experimental Procedures and Reagents

Immunoprecipitation and immunoblotting were performed according to standard procedures (Shinjyo et al., 2001) using 2% gelatin as a blocking agent. Mass spectrometry was performed by methods described in the Supplemental Experimental Procedures. Antibodies to pericentrin/kendrin,

Figure 5. Miki Induces γ-TuRC Formation in Mitotic Centrosomes

(A–C and G) Immunostaining of HeLa cells treated with siRNA indicated above for 48 hr with anti-γ-tubulin antibody. DNA was stained using Hoechst 33342 (left). Arrows or arrowheads indicate centrosomes at interphase or prometaphase, respectively (A and C). Relative fluorescence intensity of proteins indicated below in centrosomes at interphase (open bars), prometaphase (gray bars), or pseudometaphase (black bars) (right panel). To evaluate intensity, centrosomal areas were enriched by the edge of γ-tubulin staining, and the mean intensity in each was measured and the background levels subtracted. Shown is average with SD (100 centrosomes).

(D) HeLa cells (Pt) were treated with the siRNA (100 nM) indicated above for 48 hr. Shown is immunoblot analysis using antibodies indicated at left.

(E and F) HeLa cells were treated with the siRNA (100 nM) indicated above for 48 hr. Shown is immunostaining of cells at metaphase or pseudometaphase using antibodies indicated. Arrows indicate the position of mitotic centrosomes (E).

CG-NAP, and GCP2 were kind gifts of Drs. M. Takahashi and Y. Ono (Takahashi et al., 2002). Rabbit anti-Miki polyclonal antibody was described elsewhere (Asou et al., 2009). Commercial antibodies were obtained from the following suppliers: actin (1378 996) from Roche; α-tubulin (T9026) and γ-tubulin (T6557) from Sigma, tankyrase-1 (H-350) from Santa Cruz Biotechnologies, PAR (10H) from Trevigen, and p230 (#15) from BD Bioscience, ch-TOG (QED). 3-aminobenzamide was purchased from Merck; Hoechst 33342 from Invitrogen; and thymidine, aphidicolin, and nocodazole from Sigma.

SUPPLEMENTAL INFORMATION

Supplemental Information includes four figures, four movies, and Supplemental Experimental Procedures and can be found with this article at http://dx.doi.org/10.1016/j.molcel.2012.06.033.

ACKNOWLEDGMENTS

We thank Drs. N. Oshimori and N. Tokai-Nishizumi for establishment of cell lines and helpful discussion and Ms. M. Nakamura and Mr. N. Yamazaki for excellent technical assistance. This work was supported by Grants-in-Aid for Scientific Research from the Ministry of Education, Culture, Sports, Science, and Technology of Japan.

Received: November 28, 2011
Revised: February 28, 2012
Accepted: June 19, 2012
Published online: August 2, 2012

REFERENCES

Asou, H., Matsui, H., Ozaki, Y., Nagamachi, A., Nakamura, M., Aki, D., and Inaba, T. (2009). Identification of a common microdeletion cluster in 7q21.3 subband among patients with myeloid leukemia and myelodysplastic syndrome. Biochem. Biophys. Res. Commun. *383*, 245–251.

Blagden, S.P., and Glover, D.M. (2003). Polar expeditions—provisioning the centrosome for mitosis. Nat. Cell Biol. *5*, 505–511.

Brouhard, G.J., Stear, J.H., Noetzel, T.L., Al-Bassam, J., Kinoshita, K., Harrison, S.C., Howard, J., and Hyman, A.A. (2008). XMAP215 is a processive microtubule polymerase. Cell *132*, 79–88.

Chang, P., Jacobson, M.K., and Mitchison, T.J. (2004). Poly(ADP-ribose) is required for spindle assembly and structure. Nature *432*, 645–649.

Chang, P., Coughlin, M., and Mitchison, T.J. (2005a). Tankyrase-1 polymerization of poly(ADP-ribose) is required for spindle structure and function. Nat. Cell Biol. *7*, 1133–1139.

Chang, W., Dynek, J.N., and Smith, S. (2005b). NuMA is a major acceptor of poly(ADP-ribosyl)ation by tankyrase 1 in mitosis. Biochem. J. *391*, 177–184.

Chi, N.W., and Lodish, H.F. (2000). Tankyrase is a golgi-associated mitogen-activated protein kinase substrate that interacts with IRAP in GLUT4 vesicles. J. Biol. Chem. *275*, 38437–38444.

Dynek, J.N., and Smith, S. (2004). Resolution of sister telomere association is required for progression through mitosis. Science *304*, 97–100.

Gergely, F., Draviam, V.M., and Raff, J.W. (2003). The ch-TOG/XMAP215 protein is essential for spindle pole organization in human somatic cells. Genes Dev. *17*, 336–341.

Gordon, M.B., Howard, L., and Compton, D.A. (2001). Chromosome movement in mitosis requires microtubule anchorage at spindle poles. J. Cell Biol. *152*, 425–434.

Keryer, G., Di Fiore, B., Celati, C., Lechtreck, K.F., Mogensen, M., Delouvee, A., Lavia, P., Bornens, M., and Tassin, A.M. (2003). Part of Ran is associated with AKAP450 at the centrosome: involvement in microtubule-organizing activity. Mol. Biol. Cell *14*, 4260–4271.

Kuribara, R., Kinoshita, T., Miyajima, A., Shinjyo, T., Yoshihara, T., Inukai, T., Ozawa, K., Look, A.T., and Inaba, T. (1999). Two distinct interleukin-3-mediated signal pathways, Ras-NFIL3 (E4BP4) and Bcl-xL, regulate the survival of murine pro-B lymphocytes. Mol. Cell. Biol. *19*, 2754–2762.

Levesque, A.A., and Compton, D.A. (2001). The chromokinesin Kid is necessary for chromosome arm orientation and oscillation, but not congression, on mitotic spindles. J. Cell Biol. *154*, 1135–1146.

Li, C.F., MacDonald, J.R., Wei, R.Y., Ray, J., Lau, K., Kandel, C., Koffman, R., Bell, S., Scherer, S.W., and Alman, B.A. (2007). Human sterile alpha motif domain 9, a novel gene identified as down-regulated in aggressive fibromatosis, is absent in the mouse. BMC Genomics *8*, 92. http://dx.doi.org/10.1186/1471-2164-8-92.

Mauritzson, N., Albin, M., Rylander, L., Billstrom, R., Ahlgren, T., Mikoczy, Z., Bjork, J., Stromberg, U., Nilsson, P.G., Mitelman, F., et al. (2002). Pooled analysis of clinical and cytogenetic features in treatment-related and de novo adult acute myeloid leukemia and myelodysplastic syndromes based on a consecutive series of 761 patients analyzed 1976-1993 and on 5098 unselected cases reported in the literature 1974-2001. Leukemia *16*, 2366–2378.

Mishima, M., Pavicic, V., Gruneberg, U., Nigg, E.A., and Glotzer, M. (2004). Cell cycle regulation of central spindle assembly. Nature *430*, 908–913.

Nigg, E.A. (2002). Centrosome aberrations: cause or consequence of cancer progression? Nat. Rev. Cancer *2*, 815–825.

Oshimori, N., Ohsugi, M., and Yamamoto, T. (2006). The Plk1 target Kizuna stabilizes mitotic centrosomes to ensure spindle bipolarity. Nat. Cell Biol. *8*, 1095–1101.

Oshimori, N., Li, X., Ohsugi, M., and Yamamoto, T. (2009). Cep72 regulates the localization of key centrosomal proteins and proper bipolar spindle formation. EMBO J. *28*, 2066–2076.

Ozaki, Y., Matsui, H., Nagamachi, A., Asou, H., Aki, D., and Inaba, T. (2011). The dynactin complex maintains the integrity of metaphasic centrosomes to ensure transition to anaphase. J. Biol. Chem. *286*, 5589–5598.

Seimiya, H., Muramatsu, Y., Smith, S., and Tsuruo, T. (2004). Functional subdomain in the ankyrin domain of tankyrase 1 required for poly(ADP-ribosyl)ation of TRF1 and telomere elongation. Mol. Cell. Biol. *24*, 1944–1955.

Shi, Q., and King, R.W. (2005). Chromosome nondisjunction yields tetraploid rather than aneuploid cells in human cell lines. Nature *437*, 1038–1042.

Shinjyo, T., Kuribara, R., Inukai, T., Hosoi, H., Kinoshita, T., Miyajima, A., Houghton, P.J., Look, A.T., Ozawa, K., and Inaba, T. (2001). Downregulation of Bim, a proapoptotic relative of Bcl-2, is a pivotal step in cytokine-initiated survival signaling in murine hematopoietic progenitors. Mol. Cell. Biol. *21*, 854–864.

Sillje, H.H., and Nigg, E.A. (2006). Purification of mitotic spindles from cultured human cells. Methods *38*, 25–28.

Takahashi, M., Yamagiwa, A., Nishimura, T., Mukai, H., and Ono, Y. (2002). Centrosomal proteins CG-NAP and kendrin provide microtubule nucleation sites by anchoring gamma-tubulin ring complex. Mol. Biol. Cell *13*, 3235–3245.

Tokai-Nishizumi, N., Ohsugi, M., Suzuki, E., and Yamamoto, T. (2005). The chromokinesin Kid is required for maintenance of proper metaphase spindle size. Mol. Biol. Cell *16*, 5455–5463.

Vaughan, K.T. (2005). TIP maker and TIP marker; EB1 as a master controller of microtubule plus ends. J. Cell Biol. *171*, 197–200.

Weaver, B.A., Bonday, Z.Q., Putkey, F.R., Kops, G.J., Silk, A.D., and Cleveland, D.W. (2003). Centromere-associated protein-E is essential for the mammalian mitotic checkpoint to prevent aneuploidy due to single chromosome loss. J. Cell Biol. *162*, 551–563.

Yeh, T.Y., Sbodio, J.I., and Chi, N.W. (2006). Mitotic phosphorylation of tankyrase, a PARP that promotes spindle assembly, by GSK3. Biochem. Biophys. Res. Commun. *350*, 574–579.

Zimmerman, W.C., Sillibourne, J., Rosa, J., and Doxsey, S.J. (2004). Mitosis-specific anchoring of gamma tubulin complexes by pericentrin controls spindle organization and mitotic entry. Mol. Biol. Cell *15*, 3642–3657.

bjh research paper

Identification of the integrin β3 L718P mutation in a pedigree with autosomal dominant thrombocytopenia with anisocytosis

Yoshiyuki Kobayashi,[1,2] Hirotaka Matsui,[1]* Akinori Kanai,[1] Miyuki Tsumura,[2] Satoshi Okada,[2] Mizuka Miki,[2] Kazuhiro Nakamura,[2] Shinji Kunishima,[3] Toshiya Inaba[1] and Masao Kobayashi[2]

[1]Department of Molecular Oncology and Leukaemia Programme Project, Research Institute for Radiation Biology and Medicine, Hiroshima University, [2]Department of Paediatrics, Graduate School of Biomedical and Health Sciences, Hiroshima University, Minami-ku, Hiroshima, and [3]Department of Advanced Diagnosis, Clinical Research Centre, National Hospital Organization Nagoya Medical Centre, Nagoya, Aichi, Japan

Received 29 June 2012; accepted for publication 22 October 2012

Correspondence: Hirotaka Matsui, Department of Molecular Oncology and Leukemia Program Project, Research Institute for Radiation Biology and Medicine, Hiroshima University, 1-2-3 Kasumi, Minami-ku, Hiroshima 734-8553, Japan.
E-mail: hmatsui@hiroshima-u.ac.jp

Summary

αIIbβ3 integrin mutations that result in the complete loss of expression of this molecule on the platelet surface cause Glanzmann thrombasthenia. This is usually autosomal recessive, while other mutations are known to cause dominantly inherited macrothrombocytopenia (although such cases are rare). Here, we report a 4-generation pedigree including 10 individuals affected by dominantly inherited thrombocytopenia with anisocytosis. Six individuals, whose detailed clinical and laboratory data were available, carried a non-synonymous *ITGB3* gene alteration resulting in mutated integrin β3 (ITGB3)-L718P. This mutation causes partial activation of the αIIbβ3 complex, which promotes the generation of abnormal pro-platelet-like protrusions through downregulating RhoA (RHOA) activity in transfected Chinese Hamster Ovary cells. These findings suggest a model whereby the integrin β3-L718P mutation contributes to thrombocytopenia through gain-of-function mechanisms.

Keywords: integrin β3 L718P mutation, familial thrombocytopenia, autosomal dominant inheritance, whole exome sequencing, inhibition of RhoA.

Lifelong haemorrhagic syndromes are in part caused by point mutations in the *ITGA2B* and *ITGB3* genes encoding ITGA2B and ITGB3 proteins (integrin αIIb and β3, respectively). The αIIbβ3 complex regulates thrombopoiesis by megakaryocytes and aggregation of platelets in response to extracellular stimuli, such as ADP and collagen. The autosomal recessive syndrome, Glanzmann thrombasthenia, is the most frequently encountered disease caused by αIIbβ3 mutations (George *et al*, 1990; Nurden, 2006; Nurden & Nurden, 2008; Nurden *et al*, 2011a). Patients have a homozygous or a compound heterozygous mutation in the *ITGA2B* or *ITGB3* genes that causes loss of function of the αIIbβ3 complex. Although platelet counts and size are generally normal, patients typically have severe mucocutaneous bleeding, such as epistaxis, menorrhagia and gastrointestinal bleeding, frequently because of defects in platelet aggregation.

Mutations of the αIIbβ3 complex are also involved in congenital haemorrhagic diseases other than Glanzmann thrombasthenia (Ghevaert *et al*, 2008; Schaffner-Reckinger *et al*, 2009; Jayo *et al*, 2010; Kunishima *et al*, 2011; Nurden *et al*, 2011b). For example, the integrin β3 D723H mutation is found in autosomal dominant macrothrombocytopenia (Ghevaert *et al*, 2008). Biochemical analysis revealed that integrin β3-D723H is a gain of function mutation which activates the αIIbβ3 complex constitutively, albeit only partially. This results in the formation of proplatelet-like protrusions in transfected Chinese Hamster Ovary (CHO) cells, a model of relevance for the formation of macrothrombocytes (Ghevaert *et al*, 2008; Schaffner-Reckinger *et al*, 2009).

More recently, a sporadic patient carrying an integrin β3-L718P mutation was reported (Jayo *et al*, 2010). She had mild thrombocytopenia (127×10^9/l), platelet anisocytosis and reduced platelet aggregation potential. This mutation also induces abnormal proplatelet formation.

In the present study, we report a pedigree with a total 10 of individuals affected by a dominantly inherited haemorrhagic

First published online 17 December 2012
doi:10.1111/bjh.12160

syndrome. Six individuals whose detailed clinical and laboratory data are available, presented with thrombocytopenia accompanied by anisocytosis and carry a non-synonymous *ITGB3* T2231C alteration resulting in the integrin β3-L718P mutation. We also performed entire exon sequencing by a next-generation sequencing and found that the integrin β3-L718P mutation is most likely the sole gene responsible for thrombocytopenia in this pedigree.

Materials and methods

Written informed consent was obtained from individuals in the family in accordance with the Declaration of Helsinki for blood sampling and analysis undertaken with the approval of the Hiroshima University Institutional Review Board.

Patient

The patient was 4-year-old Japanese girl (iv.3 in Fig 1A), who presented with mild bleeding tendencies, such as recurrent nasal bleeding and purpura in her extremities. Her platelet count was 49–72 × 10^9/l with a mean platelet volume (MPV) of 9·8–10·9 fl. White blood cell and red blood cell counts were within the normal range and there were no morphological abnormalities including inclusions in neutrophils. Bone marrow examination was not performed. A total of six of her relatives, namely her father (iii.2), sister and brother (iv.1 and iv.2), two cousins (iv.4 and iv.5) and an aunt (iii.5), were subsequently found to have low platelet counts and were referred to our institute for further investigation.

Antibodies and reagents

Unconjugated or phycoerythrin-cyanin 5 (PC5)-conjugated anti-CD41 monoclonal antibody (Ab) (clone P2) against the αIIbβ3 complex (Beckman Coulter, Brea, CA, USA), fluorescein isothiocyanate (FITC)-conjugated anti-CD41a monoclonal Ab (clone HIP8) (Beckman Coulter), FITC- or peridinin chlorophyll (PerCP)-conjugated anti-CD61 monoclonal Ab (clone RUU-PL 7F12) (BD Biosciences, San Jose, CA, USA), FITC-conjugated PAC-1 (BD Biosciences) and Alexa488-conjugated human fibrinogen (Life Technologies, Carlsbad, CA, USA) were used in flow cytometry. Anti-CD61 monoclonal Ab (clone EP2417Y) (Abcam, Cambridge, UK), anti-DDDDK-tag polyclonal Ab (Medical & Biological Laboratories, Nagoya, Japan), Alexa488-conjugated phalloidin and Hoechst 33342 (both Life Technologies) were used for immunofluorescence microscopy. The oligopeptide Arg-Gly-Asp-Ser (RGDS) (Sigma–Aldrich, St Louis, MO, USA) was used to competitively inhibit the binding of ligands to αIIbβ3, and adenosine diphosphate (ADP) (nacalai tesque, Kyoto, Japan) was used for the stimulation of αIIbβ3 on platelets.

Construction and transfection of expression vectors

Full-length wild type (WT) *ITGA2B* and *ITGB3* cDNA were amplified by polymerase chain reaction (PCR) and cloned into pcDNA3·1 expression vectors. A PCR-mediated site-directed mutagenesis technique was applied to produce *ITGB3* mutants encoding integrin β3-L718P, -D723H and -T562N with or without truncation at the C-terminal side of Y^{759} (del. 759). *RHOA* cDNA, which encodes RhoA (RHOA) protein, was amplified by PCR and its mutants (T19N and Q63L) were generated by site-directed mutagenesis, followed by cloning into p3xFLAG-CMV-10 vectors (Sigma–Aldrich). The *ITGA2B* and *ITGB3* expression vectors were simultaneously transfected into CHO cells cultured in Ham's F12 medium supplemented with 10% fetal bovine serum at 37°C, in 5% CO_2, using Lipofectamine LTX reagent (Life Technologies) according to the manufacturer's instructions.

Immunofluorescent laser-scanning confocal microscopy

Cells grown on coverslips coated with 100 μg/ml fibrinogen were fixed with 4% paraformaldehyde, followed by permeabilization with phosphate-buffered saline containing 0·1% Triton X100. After blocking, the cells were stained with primary antibodies at appropriate dilutions, followed by staining with Alexa488- or Cy3-conjugated secondary antibodies together with Hoechst 33342. High-resolution immunofluorescent images were taken under a laser-scanning confocal microscopy (LSM5 Pascal, Carl Zeiss, Oberkochen, Germany) using a x63 objective.

Flow cytometry

The expression and activation of integrin αIIb and β3 on the platelet surface was indirectly estimated by flow cytometry with the antibodies described above. Mean fluorescence intensity (MFI) of values in an affected individual were divided by those in an unrelated normal control and recorded as relative MFI value (%). For the quantitative determination of αIIbβ3 molecules on the platelet surface, QIFIKIT (Dako, Glostrup, Denmark) was used according to the manufacturer's instructions. MFI of the calibration beads containing five populations (antibody-binding capacity: 2600, 9900, 46 000, 221 000 and 741 000) were 16·12, 63·83, 262·84, 1483·2 and 3772·1, respectively, whereas that of the negative control sample was 1·62. Therefore, αIIbβ3 molecules (copies/platelet) was calculated as $10^{(1·022 \times \log(\mathrm{MFI}) + 2·1679)} - 241$. Activation of platelets and CHO cells was estimated by methods previously described (Shattil *et al*, 1987; Hughes *et al*, 1996). Activation index was defined as $(F-F_0) / (F'-F_0)$, where F is the MFI of PAC-1-stained CHO cells transfected with αIIbβ3-L718P or αIIbβ3-D723H, and F_0 and F' are those transfected with αIIbβ3-WT and αIIbβ3-T562N, respectively. The samples were analyzed on a FACS Calibur (Becton Dickinson, Franklin Lakes, NJ, USA), equipped with an argon laser operating at 488 nm.

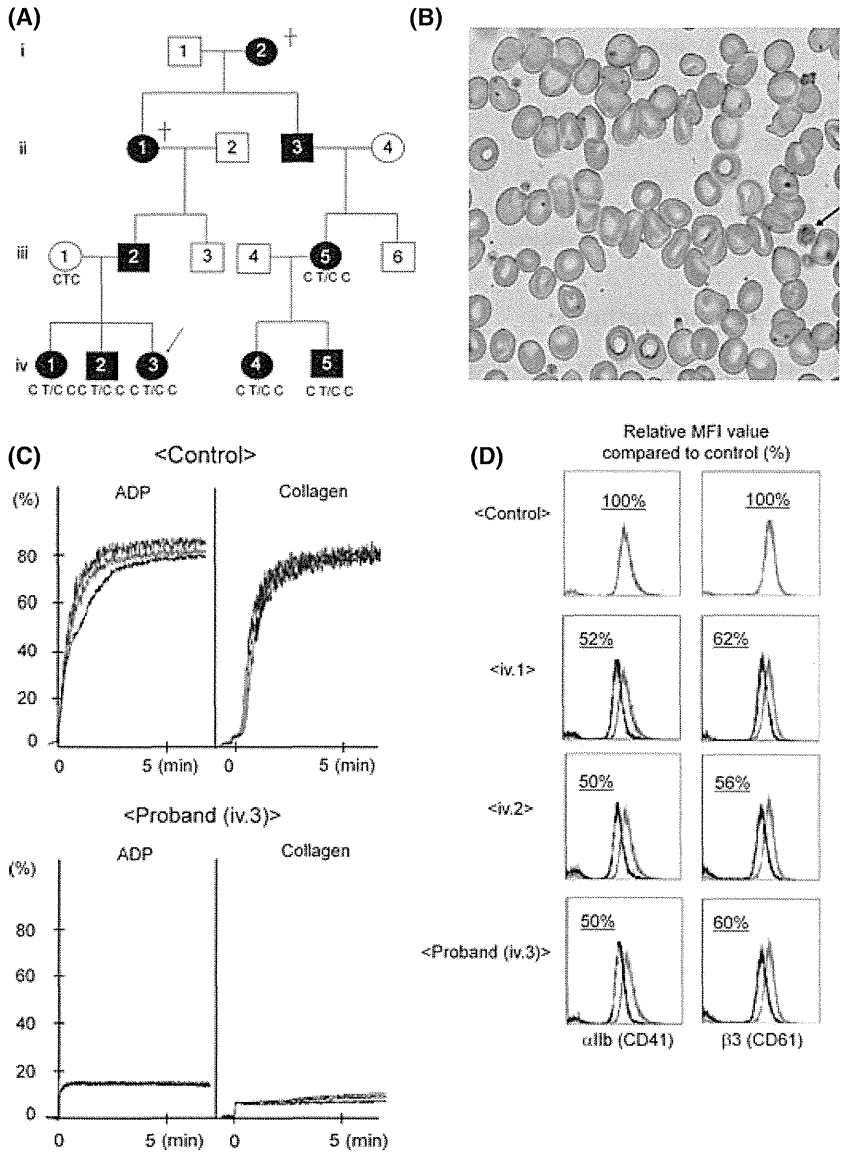

Fig 1. Platelet morphology and aggregation tracings. (A) The pedigree shows affected (filled) and unaffected (open) females (circles) and males (squares). The patient is indicated by an arrow. (B) Platelet morphology as determined by optical microscopy. Peripheral blood specimen obtained from the patient stained with May-Giemsa. The arrow indicates a macrothrombocyte. Original magnification × 600. (C) Representative platelet aggregation tracings in response to ADP and collagen stimuli in platelet-rich plasma from the patient and an unrelated normal control. (D) Flow cytometry of surface integrin αIIb (CD41) and β3 (CD61) expression. Samples were obtained from three affected individuals of the pedigree and an unrelated normal control. Data were calculated as relative MFI value (%), where MFIs of affected individuals were divided by MFI of a control sample.

Exome sequencing

Genomic DNA was obtained from four affected individuals in the pedigree and whole exome sequencing was performed. Briefly, 3 μg genomic DNA was fragmented by Covaris S2 (Covaris, Woburn, MA, USA) and ligated to adaptors, followed by hybridization to biotinylated RNA baits according to the manufacturer's instruction (Agilent Technologies, Santa Clara, CA, USA). The generated sequence tags were sequenced by the 76 bp paired-end protocol of Illumina GAIIx (Illumina, San Diego, CA, USA) and mapped onto the human genomic sequence (hg18, UCSC Genome Browser) using the sequence alignment program Eland (Illumina). Unmapped or redundantly mapped sequences were removed from the data set, and only uniquely mapped sequences were used for further analyses. Positions relative to RefSeq genes were calculated based on the respective genomic coordinates. Genomic coordinates of exons and the protein-coding regions of the RefSeq transcripts are as described in hg18. To verify the presence of *ITGB3* gene alteration, amplification and direct sequencing of a part of exon 14 was performed with the following primers; 5′-CATAGCCAGTTCAAGTGACTCCTG-3′ for forward primer and 5′-ACGATGGTACTGGCTGAACATGAC-3′ for reverse primer.

Results

Pedigree of a family with autosomal dominant thrombocytopenia with anisocytosis

In the original patient, marked platelet anisocytosis was observed in peripheral blood samples (Fig 1B). Platelet aggregation induced by ADP (1–4 μmol/l) and collagen (0·5–2 μg/ml) was markedly reduced (Fig. 1C and Table I), but agglutination induced by ristocetin (1·25 mg/ml) was within

the normal range (data not shown). Three affected individuals (iii.5, iv.1, and iv.2) showed abnormalities in platelet function similar to those of the original patient. In these affected individuals, the αIIb and β3 expression levels, which were indirectly estimated as relative MFI value (%), were 43–75% of a healthy control (Fig 1D and Table I). The number of αIIbβ3 molecules on the platelet surface in patients, as evaluated by flow cytometry using QIFIKIT, was 35 000–38 400 copies/platelet (MFI: 212·1 –232·4), whereas in an unaffected individual of the pedigree (iii.1) and an unrelated control, there were 65 200 and 62 100 copies/platelet (MFI: 389·2 and 371·3), respectively (Table I). The tendency to bleed was mild to moderate, as exemplified by the following episodes: when family member iv.1 received a bruise to the face, treatment with recombinant Factor VIIa was required because of persistent epistaxis; also, family member iii.5 had had to give birth by Caesarean section because of low platelet count. The family pedigree (Fig 1A), which shows no evidence of consanguineous marriage, strongly suggests the inheritance of thrombocytopenia as an autosomal dominant trait. The laboratory findings are shown in Table I.

Identification of the integrin β3 L718P mutation by whole exome analysis

To isolate a candidate gene alteration responsible for the thrombocytopenia, whole exome sequencing analysis was performed using genomic DNA obtained from the patient (iv.3), her sister and brother (iv.1 and iv.2) and a cousin (iv.4). A total of 794 non-synonymous gene alterations among 1551 SNPs that are not registered in dbSNP 129/130 were detected in the patient. To isolate the responsible gene, we selected non-synonymous gene alterations shared by the four affected individuals as strong candidates. Among the 90 alterations commonly found in the affected individuals of the pedigree (individual numbers of SNPs/mutations are shown in Table II), we focused on the heterozygous non-synonymous T2231C alteration in exon 14 of the *ITGB3* gene, which results in the substitution of leucine at 718 for proline (L718P) in the integrin β3 protein. We selected this because it was recently reported as a candidate mutation responsible for thrombocytopenia (Jayo *et al*, 2010). The presence of the mutation in six affected individuals of the pedigree (iv.1, iv.2, iv.3, iv.4, iii.5 and iv.5) and its absence in an unaffected individual (iii.1) and an unrelated control was confirmed by a direct-sequencing (Fig 2). As far as we could determine, no other non-synonymous gene alterations previously reported to cause thrombocytopenia or defective platelet function were present in the affected individuals of the pedigree. In addition, the L718 residue in integrin β3 is well-conserved between species and amino acid substitution in this position is predicted by bioinformatic tools, including Polyphen and SIFT, to cause a significant change in protein structure and function (data not shown). These observations strongly suggest that the L718P mutation in integrin β3 is the responsible gene alteration that causes familial thrombocytopenia.

Constitutive but partial activation of the αIIbβ3 complex by β3-L718P

To elucidate the effects of the integrin β3-L718P mutation on the activation status of αIIbβ3 complexes in resting or ADP-activated platelets, fresh platelets were analysed by flow cytometry using PAC-1, a ligand-mimicking antibody that specifically recognizes the activated form of the αIIbβ3 complex (Shattil *et al*, 1987).

Resting control platelets from healthy individuals bound PAC-1 with a similar affinity to those treated with RGDS, a peptide which competitively inhibits the binding of ligands for

Table I. Laboratory data of seven individuals of the pedigree.

						Relative MFI value compared to control (%)		αIIbβ3 molecules		Platelet aggregation (%)	
Patient	Sex	Age (years)	Platelet count ($\times 10^9$/l)	MPV (fl)	PDW (%)	αIIb	β3	MFI	copies/platelet	ADP (4 μM)	collagen (2·0 μg/ml)
iii.1	F	37	210	10·2	12·1	110	111	389·2	65 200	NA	NA
iii.5	F	34	38–67	8·5–11·3	10·0–19·0	43	75	NA	NA	15	12
iv.1	F	11	30–43	7·8–11·2	9·7–16·3	52	62	232·4	38 400	16	8
iv.2	M	8	49–64	10·3–11·1	10·1–14·7	50	56	216·4	35 700	23	16
iv.3	F	6	49–72	9·8–10·9	11·1–13·3	50	60	212·1	35 000	12	8
iv.4	F	4	32–59	9·9–10·8	12·3–15·6	NA	NA	NA	NA	NA	NA
iv.5	M	2	28–50	8·9–9·0	18·0–18·4	49	51	NA	NA	NA	NA

MPV, mean platelet volume (normal range: 9·4–12·3 fl); PDW, platelet distribution width (normal range: 9·5–14·8 %); NA, not available. αIIbβ3 molecules (copies/platelet) were calculated as $10^{(1.022 \times \log(\mathrm{MFI}) + 2.1679)} - 241$ (see *Materials and methods*).

Table II. Number of SNPs/mutations detected by whole exome sequencing.

Case	iv.1	iv.2	iv.3	iv.4
SNP	21 531	21 697	20 413	20 113
Not in dbSNP 129 and 130	1 674	1 722	1 473	1 551
Non-synonymous alternations				
Homozygous	62	58	65	42
Heterozygous	800	815	667	752
Non-synonymous (common)	90			

αIIbβ3 complex such as fibrinogen and PAC-1 (Fig 3A, compare black and blue lines), indicating that wild-type αIIbβ3 in resting platelets is not activated. In contrast, platelets obtained from the affected individuals (iii.5, iv.1, iv.2 and iv.3) showed a slight increase of PAC-1 binding compared to those treated with RGDS (Fig 3A). Indeed, resting platelets from affected individuals showed a slight but significant increase of PAC-1 binding relative to healthy individuals (Fig 3A, top panel). In addition, flow cytometric analysis using FITC-conjugated fibrinogen also showed a significant increase of fibrinogen binding potential in resting platelets from affected individuals compared with healthy controls (bottom panel). Because MPV (shown in Table I) did not exceed the normal range (9·4–12·3 fl) and surface expression levels of αIIbβ3 were lower in patients than controls (Fig 1D), it is proposed that these observations indicate spontaneous activation of αIIbβ3-L718P in resting platelets.

ADP-activated platelets from healthy volunteers, on the other hand, bound to PAC-1 with a very high affinity (Fig 3B, red lines and 3B, top panel), as expected. In contrast, only a small increase of affinity to PAC-1 was observed in ADP-treated platelets carrying the β3-L718P mutation, resulting in a marginal increase of binding potential (bottom panel). These findings suggest that αIIbβ3-L718P is partially activated in the absence of inside-out signals such as ADP, but nevertheless cannot be fully activated in the presence of such signals.

To confirm the contribution of the integrin β3-L718P mutation to spontaneous activation of αIIbβ3, CHO cells were transiently transfected with expression vectors encoding integrin β3-WT, -L718P, -D723H or -T562N together with a vector encoding αIIb-WT. Flow cytometric analysis (Fig 3C) revealed that αIIbβ3-L718P expressed in CHO cells bound to PAC-1 to the same degree as αIIbβ3-D723H, a mutant previously reported to partially activate αIIbβ3, and to a lesser extent than a fully active αIIbβ3-T562N mutant (Kashiwagi *et al*, 1999). We calculated the activation indices (see *Materials and methods*) (Hughes *et al*, 1996; Schaffner-Reckinger *et al*, 2009) of αIIbβ3-L718P and -D723H as 0·23 ± 0·07 and 0·16 ± 0·02, respectively, taking αIIbβ3-T562N as fully active (=1·0) and αIIbβ3-WT as inactive (=0) (Fig 3D). Because CHO cells were not stimulated by ADP in this experiment, each index represents αIIbβ3 activation status at rest.

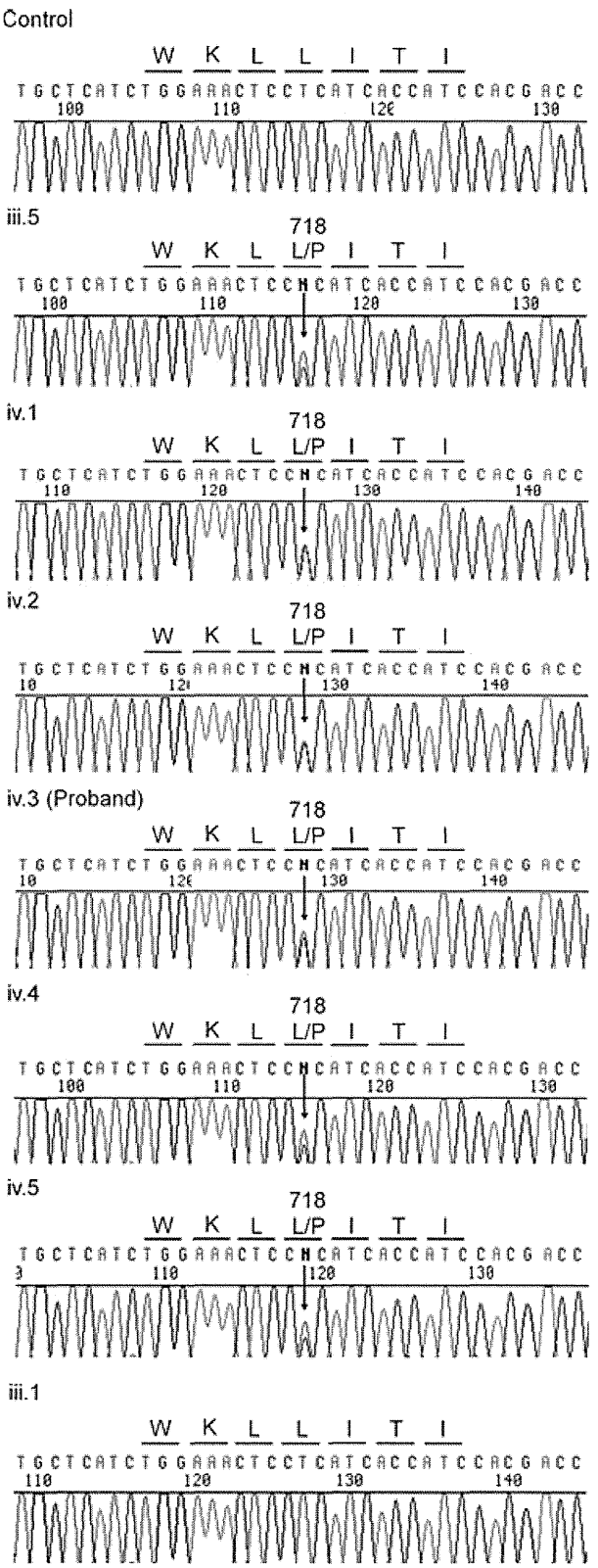

Fig 2. Direct sequencing analysis around T2231 in exon 14 of the *ITGB3* gene. Genomic DNA extracted from the affected and unaffected individuals of the pedigree were amplified by polymerase chain reaction and sequenced. Arrows indicate the position of the T2231 mutation in the *ITGB3* gene.

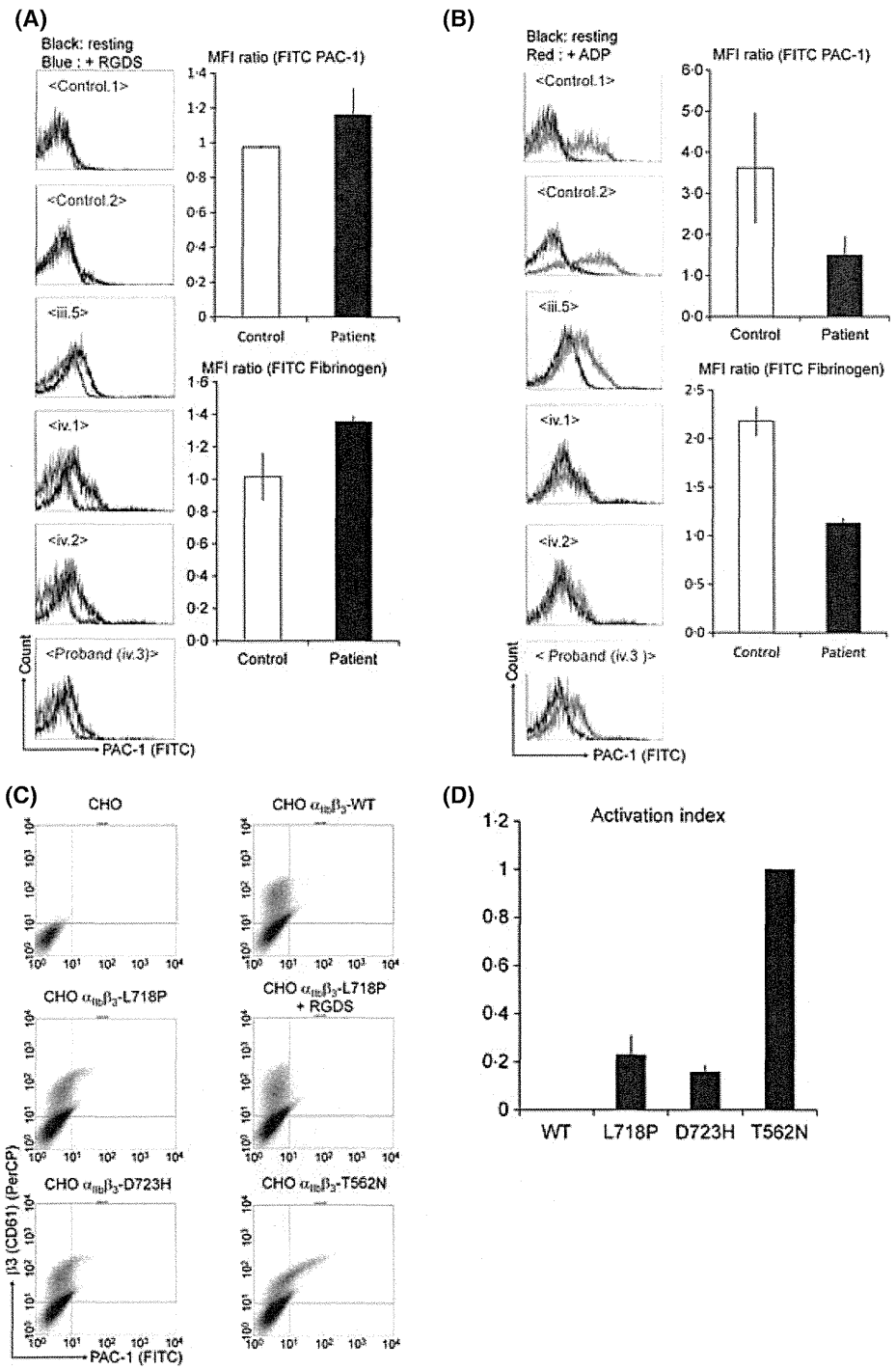

Fig 3. Functional analysis of integrin β3-L718P mutation. (A) Spontaneous binding of PAC-1 antibody to platelets obtained from affected individuals of the pedigree. Non-activated platelets (within 10 min after blood collection), incubated with or without 1 mM RGDS, were stained with FITC-conjugated PAC-1 antibody. After fixation, binding of PAC-1 to platelets was analysed by flow cytometry. Activation status of αIIbβ3 complex on resting platelets bound to FITC-PAC-1 (top) and FITC-fibrinogen (bottom). Mean fluorescence intensity (MFI) ratio was estimated by dividing the MFI of resting platelets by that of resting platelets incubated with RGDS. (B) Reduced activation of αIIbβ3 from affected individuals. The resting and ADP-stimulated platelets, stained with FITC-conjugated PAC-1 antibody were analysed by flow cytometry. Activation status of αIIbβ3 on stimulated platelets bound to FITC-PAC-1 (top) and FITC-fibrinogen (bottom). Values were estimated by dividing the MFI of platelets stimulated with ADP by those of resting platelets. (C) Partial activation of αIIbβ3-L718P and -D723H on CHO cells. CHO cells transfected with αIIbβ3 expression vectors (β3-WT, -L718P, -D723H and -T562N) were seeded on 100 μg/ml fibrinogen-coated coverslips in 6-well dishes. The cells, treated with or without RGDS, were stained with FITC-conjugated PAC-1 antibody and PerCP-conjugated anti-CD61 antibody and analysed by flow cytometry. (D) Activation index of αIIbβ3 mutants. Activation status of CHO cells expressing αIIbβ3-L718P and -D723H was compared with that of αIIbβ3-T562N as described in the "*Materials and methods*".

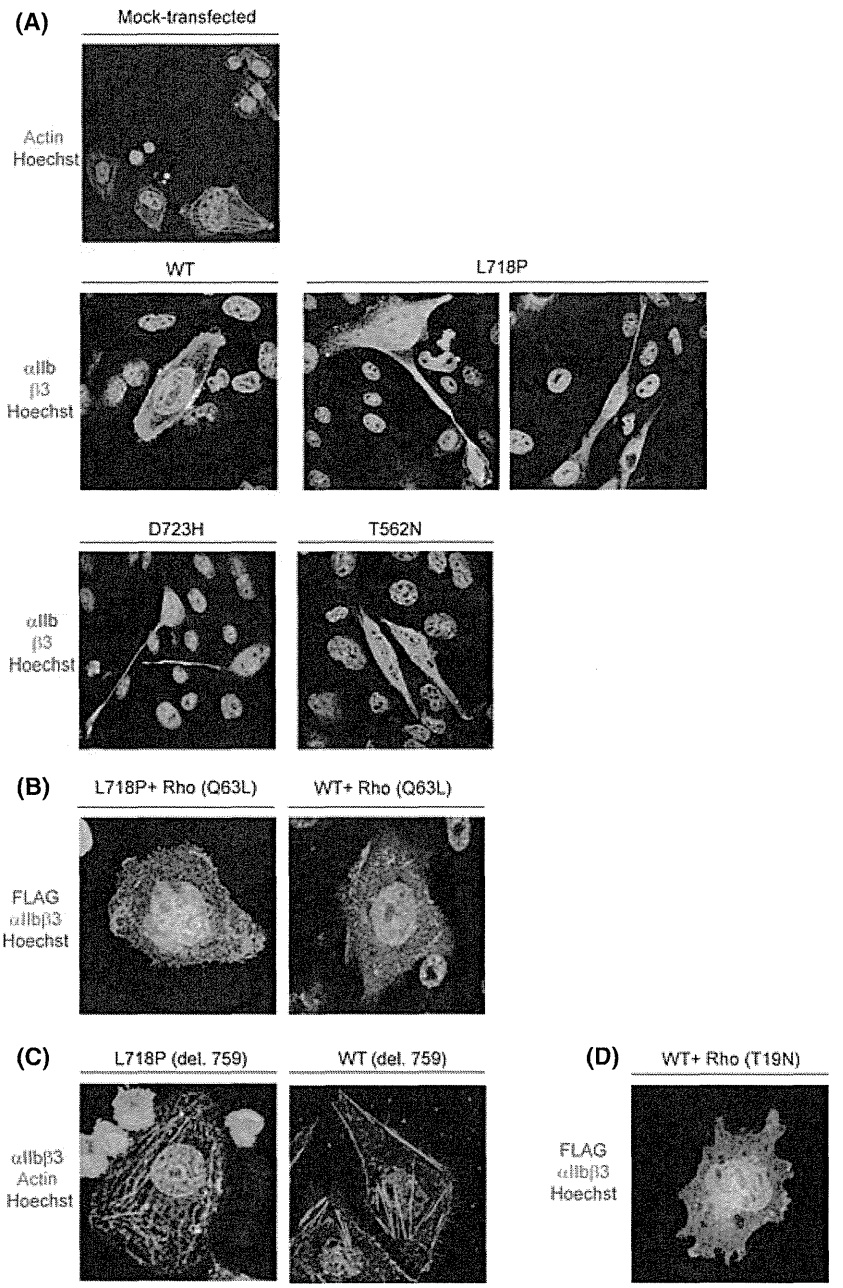

Fig 4. Overexpression of RhoA mutants or integrin β3-L718P (del. 759) modulates the formation of proplatelet-like cell protrusions in CHO cells. (A) Changes in CHO cell morphology by αIIbβ3 mutants. CHO cells transfected with αIIbβ3-L718P, -T562N and -D723H were seeded on fibrinogen-coated coverslips. After an 8-h incubation, the cells were fixed and stained with anti-CD41 and -CD61 antibodies followed by staining with Cy3- and Alexa 488-conjugated secondary antibodies. Mock-transfected cells were stained with Alexa 488-conjugated phalloidin and Hoechst 33342. (B) Inhibition of proplatelet-like protrusion formation by constitutively-active RhoA. An expression vector that encodes FLAG-tagged RhoA (Q63L) was transfected together with αIIbβ3-L718P or -WT expressing vectors into CHO cells. The cells grown on fibrinogen-coated coverslips were fixed and stained with anti-CD41 and anti-DDDDK-tag antibodies followed by staining with Alexa 488- and Cy3-conjugated secondary antibodies. (C) C-terminal deletion of β3-L718P inhibits the formation of proplatelet-like protrusions. C-terminal deleted integrin β3-L718P or -WT (del. 759) was expressed together with αIIb in CHO cells. The cells were fixed and stained with anti-CD41 antibody followed by staining with Cy3-conjugated secondary antibody and Alexa-488-labeled phalloidin. (D) A dominant-negative (T19N) form of RhoA was overexpressed in CHO cells. Images were taken as in (B).

Involvement of RhoA signalling in proplatelet-like protrusion formation

As previously reported by others (Ghevaert *et al*, 2008; Jayo *et al*, 2010), CHO cells expressing αIIbβ3-L718P, as well as αIIbβ D723H, formed long proplatelet-like protrusions on fibrinogen-coated dishes that were not observed in cells expressing wild-type αIIbβ3 (Fig 4A). In contrast, although cells expressing αIIbβ3-T562N, which yields a fully activated conformation (Kashiwagi *et al*, 1999), changed from their original round shape surrounded by a broad protrusion (Fig 4A, mock-transfected) to rhomboid-like cell morphology, proplatelet-like protrusions were rarely seen (Fig 4A). This suggests that mutants partially activating the integrin complex induce long proplatelet-like protrusions.

Recently, it was reported that the formation of proplatelet-like protrusions in CHO cells is mediated by the downregulation of RhoA activity (Chang *et al*, 2007; Schaffner-Reckinger *et al*, 2009), which is initiated by the binding of c-Src to the C-terminal tail (amino acid 760–762, Arg-Gln-Thr; RGT) of integrin β3 (Flevaris *et al*, 2007). We found that the formation of long cell protrusions was inhibited when a constitutively-active form of RhoA (Q63L) was introduced into αIIbβ3-L718P-expressing cells (Fig 4B). In addition, CHO cells expressing αIIbβ3-L718P (del. 759) mutant, which lacks the C-terminal c-Src binding site of in-

tegrin β3 (RGT), did not form any proplatelet-like protrusions (Fig 4C). Given that enforced activation of RhoA caused by introducing RhoA (Q63L), as well as de-repression of RhoA through C-terminal deletion of β3 in cells expressing αIIbβ3-WT, did not induce morphological changes in CHO cells (Figs 4B, C), it is proposed that constitutive inhibition but not activation through the c-terminal of β3 is responsible for the formation of abnormal cell protrusions in L718 mutants. However, as the enforced expression of a dominant negative form of RhoA (T19N) in αIIbβ3-WT expressing cells did not result in typical proplatelet-like protrusions (Fig 4D), this suggests that downregulation of RhoA was required but not sufficient for the formation of proplatelet-like protrusions induced by integrin β3-L718P.

Discussion

We report a pedigree with individuals suffering from a lifelong haemorrhagic syndrome, all of whom were carrying the integrin β3-L718P mutation. This had previously been reported only in a sporadic patient (Jayo *et al*, 2010). Next-generation sequencing, together with the clinical data of the patients, established that this integrin β3-L718P mutation causes thrombocytopenia resembling the disease caused by a different integrin mutation, β3-D723H, although the size of the platelets seems to differ somewhat between these mutations (Ghevaert *et al*, 2008; Schaffner-Reckinger *et al*, 2009).

Considering the dominant inheritance pattern of the haemorrhagic tendency caused by integrin β3-L718P as well as β3-D723H, these would be gain of function mutations, unlike those causing Glanzmann thrombasthenia. Indeed, expression of integrin β3-D723H partially activates the αIIbβ3 complex, resulting in downregulation of RhoA activity and induction of microtubule-dependent proplatelet-like cell protrusions considered relevant for production of macrothrombocytes (Ghevaert *et al*, 2008; Schaffner-Reckinger *et al*, 2009). Integrin β3-L718P appears to act in a similar fashion (Fig 4A and B). Interestingly, we demonstrate that the three C-terminal amino acid residues (RGT) of integrin β3 are required for L718P to form proplatelet-like cell protrusions (Fig 4C). RGT provides a binding site for c-Src tyrosine kinase, which was shown to inactivate RhoA (Flevaris *et al*, 2007), further supporting the hypothesis that integrin β3-L718P plays a role in causing megakaryocytes to produce abnormal platelets through the inhibition of RhoA.

In platelets derived from megakaryocytes that carry the integrin β3-L718P mutation, full activation of αIIbβ3 complex in response to inside-out stimuli is inhibited, as shown by reduced binding of PAC-1 and fibrinogen on stimulation with ADP (Fig 3B). A simple scenario is that, in platelets, integrin β3-L718P acts as a loss of function mutation. However, given that the carriers of Glanzmann's thrombasthenia who have both normal and mutant allele and express reduced amounts of the αIIbβ3 complex, in general show normal platelet aggregation, it is possible that the integrin β3-L718P mutation gains a function that ultimately results in the reduction of inside-out signals.

In summary, identification of a pedigree showing autosomal dominant inheritance leads to a model whereby the integrin β3-L718P mutation contributes to thrombocytopenia accompanied by anisocytosis most likely through gain-of-function mechanisms. Further investigations are necessary to fully elucidate these mechanisms by which this mutation exerts its abnormal effect on thrombocytosis and platelet aggregation.

Acknowledgements

We thank Prof. M. Matsumoto and Ms. M. Sasatani for providing clinical data; Ms. M. Nakamura, Ms. E. Kanai and Ms. R. Tai for excellent technical assistance. This work was partly supported by Grants-in-Aid for Scientific Research from the Ministry of Health, Labour and Welfare of Japan.

Author contributions

H.M., T.I. and M.K. designed the work. Y.K., H.M., A.K., S.O. and M.T. performed experiments and analysed data. S.K. contributed essential materials and interpreted data. M.M and K.N. contributed clinical materials and data. H.M, Y.K. and T.I. wrote the manuscript.

Conflict of interest

The authors declare no competing financial interests.

References

Chang, Y., Auradé, F., Larbret, F., Zhang, Y., Couedic, J.P.L., Momeux, L., Larghero, J., Bertoglio, J., Louache, F., Cramer, E., Vainchenker, W. & Debili, N. (2007) Proplatelet formation is regulated by the Rho/ROCK pathway. *Blood*, **109**, 4229–4236.

Flevaris, P., Stojanovic, A., Gong, H., Chishti, A., Welch, E. & Du, X. (2007) A molecular switch that controls cell spreading and retraction. *Journal of Cell Biology*, **179**, 553–565.

George, J.N., Caen, J.P. & Nurden, A.T. (1990) Glanzmann's thrombasthenia: the spectrum of clinical disease. *Blood*, **75**, 1383–1395.

Ghevaert, C., Salsmann, A., Watkins, N.A., Schaffner-Reckinger, E., Rankin, A., Garner, S.F., Stephans, J., Smith, G.A., Debili, N., Vainchenker, W.de, Groot, P.G., Huntington, J.A., Laffan, M., Kieffer, N. & Ouwehand, W.H. (2008) A non-synonymous SNP in the ITGB3 gene disrupts the conserved membrane-proximal cytoplasmic salt bridge in the αIIbβ3 integrin and cosegregates dominantly with abnormal proplatelet formation and macrothrombocytopenia. *Blood*, **111**, 3407–3414.

Hughes, P.E., Diaz-Gonzalez, F., Leong, L., Wu, C., McDonald, J.A., Shattil, S.J. & Ginsberg, M. H. (1996) Breaking the integrin hinge. A defined structural constraint regulates integrin signaling. *Journal of Biological Chemistry*, **271**, 6571–6574.

Jayo, A., Conde, I., Lastres, P., Martinez, C., Rivera, J., Vicente, V. & Manchón, C.G. (2010) L718P mutation in the membrane-proximal

cytoplasmic tail of β3 promotes abnormal αIIbβ3 clustering and lipid domain coalescence, and associates with a thrombasthenia-like phenotype. *Haematologica*, **95**, 1158–1166.

Kashiwagi, H., Tomiyama, Y., Tadokoro, S., Honda, S., Shiraga, M., Mizutani, H., Honda, M., Kurata, Y., Matsuzawa, Y. & Shattil, S.J. (1999) A mutation in the extracellular cysteine-rich repeat region of the β3 subunit activates integrins αIIbβ3 and αVβ3. *Blood*, **93**, 2559–2568.

Kunishima, S., Kashiwagi, H., Otsu, M., Takayama, N., Eto, K., Onodera, M., Miyajima, Y., Takamatsu, Y., Suzumiya, J., Matsubara, K., Tomiyama, Y. & Saito, H. (2011) Heterozygous ITGA2B R995W mutation inducing constitutive activation of the αIIbβ3 receptor affects proplatelet formation and causes congenital macrothrombocytopenia. *Blood*, **117**, 5479–5484.

Nurden, A.T. (2006) Glanzmann thrombasthenia. *Orphanet Journal of Rare Diseases*, **1**, 10.

Nurden, P. & Nurden, A.T. (2008) Congenital disorders associated with platelet dysfunctions. *Thrombosis and Haemostasis*, **99**, 253–263.

Nurden, A.T., Fiore, M., Nurden, P. & Pillois, X. (2011a) Glanznmann thrombasthenia: a review of ITGA2B and ITGB3 defects with emphasis on variants, phenotype variability, and mouse models. *Blood*, **118**, 5996–6005.

Nurden, A.T., Pillois, X., Fiore, M., Heilig, R. & Nurden, P. (2011b) Glanzmann thrombasthenia-like syndromes associated with macrothrombocytopenias and mutations in the gene encosing the αIIbβ3 integrin. *Seminars in Thrombosis and Hemostasis*, **37**, 698–706.

Schaffner-Reckinger, E., Salsmann, A., Debili, N., Bellis, J., Demey, J., Vainchenker, W., Ouwehand, W.H. & Kieffer, N. (2009) Overexpression of the partially activated αIIbβ3D723H integrin salt bridge mutant downregulates RhoA activity and induces microtubule-dependent proplatelet-like extensions in Chinese hamster ovary cells. *Journal of Thrombosis and Haemostasis*, **7**, 1207–1217.

Shattil, S.J., Cunningham, M. & Hoxie, J.A. (1987) Detection of activated platelets in whole blood using activation-dependent monoclonal antibodies and flow cytometry. *Blood*, **70**, 307–315.

Leukemia & Lymphoma, August 2012; 53(8): 1599–1609

ISSN: 1042-8194 print / 1029-2403 online
DOI: 10.3109/10428194.2012.663086

informa
healthcare

ORIGINAL ARTICLE: RESEARCH

Aberrant methylation and decreased expression of the *RIZ1* gene are frequent in adult acute lymphoblastic leukemia of T-cell phenotype

Hanae Shimura[1], Naoki Mori[1], Yan-Hua Wang[1], Michiko Okada[2] & Toshiko Motoji[1]

[1]*Department of Hematology, Tokyo Women's Medical University, Tokyo, Japan and* [2]*Chromosome Laboratory, Shiseikai Daini Hospital, Tokyo, Japan*

Abstract

Retinoblastoma protein-interacting zinc finger, *RIZ1*, is a tumor suppressor gene that is inactivated in various solid tumors. However, the role of the *RIZ1* gene has not been well examined in adult acute lymphoblastic leukemia (ALL). We analyzed the expression and promoter methylation status of the *RIZ1* gene in patients with newly diagnosed ALL by quantitative real-time reverse transcription polymerase chain reaction (PCR) and methylation-specific PCR, respectively. *RIZ1* expression in 67 cases of ALL (mean 1.043) was decreased compared with that in normal bone marrow (mean 1.471) ($p = 0.030$). Methylation was detected in 11 of 71 patients (15.5%) but not in healthy controls. Methylation was associated with decreased *RIZ1* expression in many ALL cases examined, but this was not statistically significant. In T-ALL, *RIZ1* methylation was more frequent (63.6%) than in B-ALL (6.7%) ($p < 0.0001$) and the decrease of *RIZ1* expression was more significant than in B-ALL ($p = 0.045$). 5-Aza-2′-deoxycytidine treatment of MOLT-4 cells with *RIZ1* methylation induced demethylation of *RIZ1* and restoration of expression. Forced *RIZ1* expression in T-ALL cell lines suppressed cell growth accompanied by G2/M arrest and apoptosis. No mutations were found by PCR-single strand conformation polymorphism analysis in hotspots of the gene. These results suggest that *RIZ1* is inactivated in adult ALL, and this inactivation is associated with methylation in T-ALL.

Keywords: Acute lymphoblastic leukemia, methylation, RIZ1, tumor suppressor gene, epigenetics

Introduction

Retinoblastoma protein-interacting zinc finger gene, *RIZ*, was originally isolated in functional screening for retinoblastoma-binding proteins [1]. RIZ was also independently isolated as a GATA-3-binding protein [2] and a DNA-binding protein [3]. RIZ has characteristics of a negative regulator of tumorigenesis and is considered to be a candidate tumor suppressor.

The *RIZ* gene produces two proteins: RIZ1, a positive regulatory (PR) domain plus product, and RIZ2, a PR domain-minus product. RIZ2 is otherwise identical to RIZ1, and both proteins contain the C-terminal (CR) domain [4]. The PR domain of RIZ1 is important for transcriptional repression [5], and tumor suppressor activity is localized to the PR domain, suggesting that RIZ1 but not RIZ2 has tumor suppressive properties. Forced expression of the *RIZ1* gene causes apoptosis and cell cycle arrest at G2/M and suppresses tumorigenicity in nude mice [6]. *RIZ1* knockout mice have a high incidence of diffuse large B-cell lymphoma (DLBCL) and a broad spectrum of unusual tumors [7]. *RIZ1* expression but not *RIZ2* expression has been found to be reduced in many types of human cancer, including breast cancer, lung cancer [6], colon cancer and ovarian cancer [8].

RIZ1 is inactivated as a result of a frameshift in colorectal cancers and endometrial cancers with microsatellite instability [8,9], missense mutations in DLBCL [7] and deletion of the short arm of chromosome 1 (1p), to which the gene is mapped. Furthermore, *RIZ1* promoter methylation is frequently found in gastric cancer [10], breast cancer and liver cancer [11].

In hematological malignancies, the roles of *RIZ1* remain undetermined. *RIZ1* expression was found to be significantly decreased in leukemia cell lines and acute myeloid leukemia (AML) [12]. It was also decreased in chronic myeloid leukemia (CML) during the transformation from chronic phase to blastic crisis [13]. A recent study revealed that its expression level was altered among World Health Organization (WHO) (2008) subtypes or risk groups in myelodysplastic syndrome (MDS) [14]. We have also reported that *RIZ1* promoter methylation was more frequent in MDS and secondary AML than in *de novo* AML [15].

Acute lymphoblastic leukemia (ALL) is a neoplasm of lymphoid progenitor cells and represents a heterogeneous group with variable clinical character and responsiveness to treatment [16,17]. It affects both children and adults, but genotypic differences are present between different age groups. In adult ALL, the expression and role of *RIZ1* have not

Correspondence: Naoki Mori, MD, PhD, Department of Hematology, Tokyo Women's Medical University, 8-1 Kawada-cho, Shinjuku-ku, Tokyo 162-8666, Japan. Tel: +81-3-3353-8111, ext. 31544. Fax: +81-3-5269-7329. E-mail: mori@dh.twmu.ac.jp

Received 31 December 2011; revised 31 December 2011; accepted 29 January 2012

been well examined. In a previous study, expression of *RIZ1* was not decreased in most patients with ALL, and elevated expression of *RIZ2* was considered to be related to leukemogenesis [12]. However, it is unclear whether overexpression of PR-minus *RIZ2* is related to leukemogenesis in ALL. Furthermore, although hypermethylation of the *RIZ1* gene has been described and epigenetic silencing is the common process behind *RIZ1* inactivation in solid tumors, the methylation status of the *RIZ1* gene has not been analyzed in adult ALL.

The aims of this study were to assess *RIZ* expression and altered methylation status in adult ALL and to clarify the association between these features and clinical characteristics.

Materials and methods

Patients and samples

A total of 73 newly diagnosed adult patients with ALL (62 B-ALL and 11 T-ALL) were included in this study. Histological criteria used for the diagnosis were those described in the French–American–British classification. Median age was 45.6 years (range 18–90) and 38 patients (52.1%) were male. The patients received chemotherapy in accordance with the Japan Adult Leukemia Study Group (JALSG) protocols [18–20], modified L17 (L17M) [21] or other protocols. Most of the patients with Philadelphia chromosome (Ph)-positive ALL (Ph+ALL) were treated with imatinib-containing induction chemotherapy. Complete remission was defined when normocellular bone marrow contained fewer than 5% leukemic blast cells and peripheral blood counts recovered to a normal level.

Bone marrow (BM) or peripheral blood (PB) was collected at diagnosis. Mononuclear cells were isolated by Ficoll-Conray gradient centrifugation (density 1.077 g/mL). The presence of more than 80% blast cells in each sample was confirmed using a cytospin preparation. Normal bone marrow (NBM) ($n = 10$) and peripheral blood (NPB) ($n = 2$) were also obtained from healthy volunteers. Normal T (NT) ($n = 3$) and B lymphocytes (NB) ($n = 3$) were isolated from peripheral lymphocytes using a magnetic cell separation system (Becton, Dickinson and Company, Franklin Lakes, NJ) with anti-CD4/anti-CD8 antibodies and anti-CD19/anti-CD20 antibodies, respectively. The presence of more than 95% separated phenotype cells in each sample was also confirmed using flow cytometry.

The present study was approved by the institutional review board and conducted in accordance with the guidelines of our institution. Written informed consent according to the Declaration of Helsinki was obtained from the patients.

Cytogenetic analysis

Chromosome preparations were Q-banded and karyotypes were described according to the International System for Human Cytogenetic Nomenclature (ISCN 2009). We classified patients by prognostic risk [22]. Briefly, the better prognosis cytogenetic group contained those with del(9p) or high hyperdiploidy. The poor prognosis cytogenetic group was defined as patients with t(9;22)(q24;q11.2), t(4;11)(q21;q23), t(8;14)(q24.1;q32), low hypodiploidy/near triploidy or complex karyotype. The intermediate group contained the others.

Genomic DNA and RNA isolation, cDNA synthesis

Genomic DNA was extracted using a QIAamp DNA Blood Mini Kit (Qiagen, Valencia, CA) following the manufacturer's protocol.

Total RNA was isolated by the guanidinium thiocyanate-phenol-chloroform extraction method, using TRIzol (Invitrogen, Carlsbad, CA). Two micrograms of total RNA was converted to single-strand cDNA using a random primer and a High Capacity cDNA Reverse Transcription Kit (Applied Biosystems, Foster City, CA). Each resulting cDNA was adjusted to the same density within a standard curve range with nuclease-free water, and stored at − 20 °C until use.

Quantitative real-time reverse transcription PCR

Quantitative real-time reverse transcription polymerase chain reaction (qRT-PCR) was performed as described previously [15]. Measurement of mRNA levels of *RIZ1* was based on the TaqMan probe method using an ABI 7500 real-time PCR system (Applied Biosystems). PR primer pairs and probes were purchased from Applied Biosystems (Hs 01030714_m1). CR primer pairs and probes were made according to a previous report [12]. Amplification of the PR region represents expression of *RIZ1* mRNA, whereas amplification of the CR region represents expression of *RIZ1* + *RIZ2*. The relative expressions of *RIZ1* and *RIZ1* + 2 were calculated using a comparative standard curve, which was made using serially diluted cDNA from a B-ALL cell line, Raji. All final measurements were normalized as the relative *RIZ1* and *RIZ1* + 2 mRNA expression levels with the *RIZ1*/*GAPDH* and (*RIZ1* + 2)/*GAPDH* average value for each sample, respectively, using human *GAPDH* (glyceraldehyde 3-phosphate dehydrogenase; Applied Biosystems) as an internal control gene.

Methylation-specific PCR

Genomic DNA was treated with bisulfite using a CpGenome DNA Modification Kit (Serologicals Corporation, Norcross, GA). The methylation-specific (MS)-PCR protocol and sequences of primers for the *RIZ1* gene were as described previously [15]. CpGenome Universal Methylated DNA (Serologicals Corporation), normal lymphocyte and double-distilled water were used as positive control, negative control and blank, respectively. All experiments were carried out five times using independent PCR products, and samples that showed methylated bands repeatedly were recognized as methylation-positive.

Single strand conformation polymorphism analysis

Missense mutation in exon 7 and frameshift mutations at $(A)_8$ and $(A)_9$ tracks in exon 8 of *RIZ1* were screened by single strand conformation polymorphism (SSCP) analysis. Genomic DNAs were amplified with biotinylated nucleotides and primers as described previously [23]. The primers were RP263 (5′-AACACATGAGGGAATGAATGAATG-3′) and RP264 (5′-ACACCCAATTCAGACCAAGCC-3′) for exon 7 and RIZA8-F (5′-GAGCTCAGCAAAATGTCGTC-3′) and RIZA9-R (5′-GTGATGAGTGTCCACCTTTC-3′) for $(A)_8$ and $(A)_9$ tracks. The PCR-SSCP protocol was as described previously [15,24]. Amplified DNA fragments were separated by electrophoresis on non-denaturing 6% polyacrylamide gels

with or without 10% glycerol. The separated DNA fragments were transferred to membranes (Amersham Hybond-N; GE Healthcare, Piscataway, NJ) and visualized by subsequent incubations with streptavidin, biotinylated alkaline phosphatase and a chemiluminescent substrate system (Phototope-star Detection kit; New England BioLabs, Beverly, MA).

Cell lines and reagents

MOLT-4, Jurkat (T-ALL cell lines), Raji and Daudi (B-ALL cell lines) were cultured in RPMI 1640 medium (Invitrogen Life Technologies, Carlsbad, CA) supplemented with 10% fetal calf serum (Life Technologies, Grand Island, NE) in 5% CO_2 at 37 °C. The relative expression levels of *RIZ1* and *RIZ1* + 2 and methylation status of the *RIZ1* gene in cells were also analyzed as mentioned above. MOLT-4 cells (1×10^5/mL) were grown for 96 h in the presence of 5-aza-2′-deoxycytidine (5-Aza-dC) (Wako, Osaka, Japan) at various concentrations (0.1, 0.5 and 3 μM). 5-Aza-dC was dissolved with dimethyl sulfoxide (DMSO). Cell viability was determined using a dye exclusion assay. Cell lysates were harvested at 24 and 96 h after treatment, and then total RNA was isolated for qRT-PCR analysis, and genomic DNA was subjected to MS-PCR. Three independent experiments were carried out.

RIZ1 transfections into T-ALL cell lines

The human RIZ1 protein expression vector p3RIZRH1, which was constructed by cloning the full-length wild-type human *RIZ1* cDNA into pcDNA3 vector, was kindly provided by Dr. Huang [7]. The Nucleofector system (Amaxa, Gaithersburg, MD) was used for transfecting plasmid into T-ALL cell lines (MOLT-4 and Jurkat) following the manufacturer's protocol and programs. Two micrograms of p3RIZRH1 were transfected into the cells and the same quantity of pcDNA3.1 vector (Invitrogen) was transfected as empty vector for the control. Total RNA and protein were isolated for qRT-PCR and Western blot analysis. Equal amounts of proteins (20 μg), extracted by a ProteoExtract Subcellular Proteome Extraction Kit (Merck KGaA, Darmstadt, Germany), were separated by electrophoresis and transferred to a polyvinylidene fluoride (PVDF) membrane. After blocking with 5% skim milk, the membranes were incubated with the primary antibodies against human RIZ1 protein (1:100 dilution; Abcam, Cambridge, UK; cat. no. 3791) overnight at 4 °C. A horseradish peroxidase-conjugated secondary antibody (Jackson Immuno Research, Inc., West Grove, PA) was used, and the bound antibody was visualized by chemiluminescence using Immobilon Western reagents (Millipore, Billerica, MA). The transfected cells were cultured for 96 h, and cell growth, cell cycle and apoptosis were analyzed. Cell cycle analysis of *RIZ1* or control plasmid transfected cells was performed as described previously [25]. Apoptosis was assayed using the annexin V-fluorescein isothiocyanate (FITC)/propidium iodine (PI) binding technique with an annexin V-FITC apoptosis detection kit (Beckman Coulter, Miami, FL).

Statistical analysis

Medians were compared using the Mann–Whitney *U*-test in the analysis of correlations between *RIZ1* expression and clinical characteristics or methylation status. Correlations between the frequency of *RIZ1* methylation and clinical characteristics or remission rates were analyzed using the χ^2 test. Spearman rank order correlations were used to assess the correlation between *RIZ1* and *RIZ1* + 2 expressions. Two-sample *t*-tests were used to evaluate differences in cell numbers between the groups of 5-Aza-dC-treated or *RIZ1*-transfected cell lines and the control groups. Analysis was performed using SPSS software. *p*-Values < 0.05 were considered statistically significant.

Results

Cytogenetic analysis of primary ALL samples

Cytogenetic data were available from 57 of the 73 patients with ALL. Twenty metaphases were evaluated. These patients were classified as follows: two in the better-prognosis, 20 in the intermediate-prognosis and 35 in the poor-prognosis group. No deletion of 1p or monosomy of chromosome 1 was present in any of the 57 patients.

Expression of the *RIZ1* gene in normal samples and leukemic cells

Relative mRNA expression levels of *RIZ1* and *RIZ1* + 2 in normal samples and cell lines are shown in Figure 1(A). *RIZ1* expression in NT (mean 6.933) was higher than that in NB (mean 3.229). A similar observation was found for *RIZ1* + 2. *RIZ1* + 2 expression in NT (mean 10.045) was higher than that in NB (mean 3.654). In three of the four lymphoid cell lines (MOLT-4, Jurkat and Daudi), both *RIZ1* and *RIZ1* + 2 expressions were markedly decreased compared with those of normal samples. In contrast, both *RIZ1* and *RIZ1* + 2 expressions in Raji were not decreased.

We next performed qRT-PCR analysis for 67 of the 73 patients whose RNA was available. Figure 1(B) shows *RIZ1* and *RIZ1* + 2 expressions in ALL in comparison with those of normal samples. *RIZ1* mRNA expression in total ALL (mean 1.043) was significantly decreased compared with that of NBM (mean 1.471) ($p = 0.030$). A similar relative decrease was also found in *RIZ1* + 2 ($p = 0.029$). When we focus on T-ALL, the expression of *RIZ1* (mean 0.606) was lower than that in NBM (mean 1.471) ($p = 0.003$) [Figure 1(C)]. In contrast, the expression of *RIZ1* in B-ALL (mean 1.145) was not significantly lower than that in NBM (mean 1.471) ($p = 0.065$). A similar observation was also found for *RIZ1* + 2 [Figure 1(C)]. *RIZ1* and *RIZ1* + 2 expressions and characteristics of patients are shown in Table I. *RIZ1* expression in patients with T-ALL (mean 0.606) was lower than that in patients with B-ALL (mean 1.145) ($p = 0.045$), although the expression in normal T-cells was higher than that in normal B-cells. Significant differences of *RIZ1* + 2 but not *RIZ1* expression were observed among different age, lactate dehydrogenase (LDH) and Ph chromosome groups. No correlations between other clinical characteristics and expressions were found.

The relationships between expressions of *RIZ1* and *RIZ1* + 2 in each ALL sample are shown in Figure 1(D). In total ALL, *RIZ1* and *RIZ1* + 2 had a positive correlation ($p < 0.01$). When the ratio of *RIZ1*/(*RIZ1* + 2) was calculated, it varied among patients and had no trend (data not shown).